

Dynamical Tides in Compact White Dwarf Binaries: Tidal Synchronization and Dissipation

Jim Fuller^{*} and Dong Lai

Center for Space Research, Department of Astronomy, Cornell University, Ithaca, NY 14853, USA

11 October 2018

ABSTRACT

In compact white dwarf (WD) binary systems (with periods ranging from minutes to hours), dynamical tides involving the excitation and dissipation of gravity waves play a dominant role in determining the physical conditions (such as rotation rate and temperature) of the WDs prior to mass transfer or binary merger. We calculate the amplitude of the tidally excited gravity waves as a function of the tidal forcing frequency $\omega = 2(\Omega - \Omega_s)$ (where Ω is the orbital frequency and Ω_s is the spin frequency) for several realistic carbon-oxygen WD models, under the assumption that the outgoing propagating waves are efficiently dissipated in outer layer of the star by nonlinear effects or radiative damping. Unlike main-sequence stars with distinct radiative and convection zones, the mechanism of wave excitation in WDs is more complex due to the sharp features associated with composition changes inside the WD. In our WD models, the gravity waves are launched just below the helium-carbon boundary and propagate outwards. We find that the tidal torque on the WD and the related tidal energy transfer rate, \dot{E}_{tide} , depend on ω in an erratic way, with \dot{E}_{tide} varying by orders of magnitude over small frequency ranges. On average, \dot{E}_{tide} scales approximately as $\Omega^5 \omega^5$ for a large range of tidal frequencies.

We also study the effects of dynamical tides on the long-term evolution of WD binaries prior to mass transfer or merger. Above a critical orbital frequency Ω_c , corresponding to an orbital period of order one hours (depending on WD models), dynamical tides efficiently drive Ω_s toward Ω , although a small, almost constant degree of asynchronization ($\Omega - \Omega_s \sim \text{constant}$) is maintained even at the smallest binary periods. While the orbital decay is always dominated by gravitational radiation, the tidal energy transfer can induce significant phase error in the low-frequency gravitational waveforms, detectable by the planned LISA project. Tidal dissipation may also lead to significant heating of the WD envelope and brightening of the system long before binary merger.

Key words: white dwarfs – hydrodynamics – waves – binaries

1 INTRODUCTION

Compact white dwarf (WD) binary systems (with orbital periods in the range of minutes to hours) harbor many interesting and unanswered astrophysical questions. An increasing number of such systems are being discovered by recent surveys (e.g. Mullally et al. 2009; Kulkarni & van Kerkwijk 2010; Steinfadt et al. 2010; Kilic et al. 2011; Brown et al. 2011; see Marsh 2011 for a review). The orbits of these systems decay via the emission of gravitational waves, which could be detected by the planned *Laser Interferometer Space Antenna (LISA)* (Nelemans 2009). Depending on the WD masses and the physics of the merger process, these merging

WD systems may produce single helium-rich sdO stars, giant stars (R CrB stars), stable mass transfer AM CVn binaries, or possibly underluminous supernovae. Most importantly, compact WD binaries in which the total mass is near the Chandrasekhar limit are thought to be the probable progenitors of type Ia supernovae upon a stellar merger at the end of the orbital decay process (Webbink 1984; Iben & Tutukov 1984). Recent studies have provided support for this “double degenerate” scenario (e.g., Gilfanov & Bogdan 2010; Di Stefano 2010; Maoz et al. 2010) and even sub-Chandrasekhar WD mergers may lead to type Ia supernovae (van Kerkwijk et al. 2010).

Prior to merger, tidal interactions may affect the properties of the binary WDs and their evolutions, including the phase evolution of the gravitational waves. Previous stud-

^{*} Email: derg@astro.cornell.edu; dong@astro.cornell.edu

ies have focused on equilibrium tides (e.g., Iben et al. 1998; Willems et al. 2010), corresponding to quasi-static deformation of the star. Such equilibrium tides are unlikely to play a role in the tidal synchronization/dissipation process. Iben et al. (1998) estimated the effect of tidal heating in the WD based on the assumption that the (spherically averaged) local heating rate is equal to the rate of rotational energy deposition required to maintain synchronization. They suggested that the binary WDs may brighten by several magnitudes before merger.

In fact, in a compact WD binary, as the orbital decay rate due to gravitational wave radiation increases rapidly with decreasing orbital period, it is not clear if tidal effects are sufficiently strong to drive the binary system toward synchronous rotation. The critical orbital period for synchronization is unknown. For this reason, the majority of recent WD merger simulations (e.g., Segretain et al. 1997; Loren-Aguilar et al. 2009; Pakmor et al. 2010,2011) have assumed the merging WDs to be non-synchronized prior to merger. However, whether the WDs are spin-synchronized may affect the merger product and the possible supernova signature: for example, the strong velocity shear between the stars upon contact would be significantly reduced for the merger of a synchronized binary. The degree of synchronization also determines the tidal luminosity of the binary prior to merger. Indeed, it is possible that tidal dissipation contributes significantly to the brightness of some of the recently observed WD binaries (e.g., Brown et al. 2011).

In a recent paper (Fuller & Lai 2011, hereafter Paper I), we used linear theory to calculate the excitation of discrete gravity modes in a WD due to the tidal gravitational field of a compact companion star (a WD, neutron star or black hole). The existence of discrete modes requires that gravity waves be reflected near the surface of the WD. In this case, tidal energy and angular momentum transfers between the WD and the binary orbit occur only during a series of resonances, when the g-mode frequency σ_α equals 2Ω (where Ω is the orbital frequency). Our calculations showed that while the dimensionless (mass-weighted) amplitude of the resonantly excited g-mode is not extremely non-linear (it approaches ≈ 0.1), the displacement associated with the mode becomes large in the outer layer of the WD where the density is low. In other words, while the mode does not reach a non-linear amplitude in the bulk interior of the star, it becomes very non-linear in the outer layers even before resonance. We concluded that tidally excited gravity waves are likely to continually damp in the outer layer of the WD, preventing the formation of discrete modes. A proper treatment of dynamical tides in binary WDs must take account of this continuous wave damping.

In this paper, we calculate the tidal excitation of gravity waves in binary WDs assuming that the waves are efficiently damped in the WD envelope. To this end, we implement an outgoing wave boundary condition near the WD surface. Unlike gravity modes (which have a set of discrete eigenfrequencies), the outgoing wave boundary condition permits the excitation of gravity waves at all frequencies, and thus allows for a continuous process of tidal dissipation. Similar calculations have been implemented for early-type stars (Zahn 1975,1977; Goldreich & Nicholson 1989) and solar-type stars (Goodman & Dickson 1998; Ogilvie & Lin 2007). In early-type stars, gravity waves are excited at the boundary be-

tween the convective core and radiative envelope, propagate outwards and dissipate in the outer envelope. In solar-type stars, gravity waves are similarly excited at the interface between the radiative core and convective envelope, but propagate inward before dissipating (via non-linear wave breaking) near the center of the star (Barker & Ogilvie 2010,2011). Unlike main-sequence stars, WDs do not contain a simple two-zone structure of convective and radiative regions, and it is not clear how and to what extent gravity waves are excited. The outgoing wave outer boundary condition allows us to calculate the rate at which energy and angular momentum are transferred to the WD as a function of orbital period. We can then calculate the orbital period at which tidal effects can compete with orbital decay due to gravitational radiation. At this orbital period, the synchronization process can begin. Furthermore, by scaling our results to rotating WDs, we can determine the WD spin period and energy dissipation rate at any orbital period.

This paper is organized as follows. In Sections 2-4 we derive the basic equations for tidally forced stellar oscillations, the boundary conditions and the tidal angular momentum and energy transfer rates. In Section 5 we discuss our numerical method and present several test calculations, where we emphasize the importance of using a self-consistent stellar model in order to obtain reliable amplitudes for tidally excited gravity waves. In Section 6 we present our numerical calculations of tidal excitations for realistic WD models. Since our numerical results reveal a complicated dependence of the tidal energy transfer rate on the tidal frequency, we examine a simple semi-analytic model in Section 7 to shed light on the mechanism of gravity wave excitation. In Section 8 we use the results of previous sections to study the long-term spin-orbit evolution of WD binaries, including spin synchronization, the tidal effect on the low-frequency gravitational radiation waveforms and tidal heating of the WDs. We conclude in Section 9 with a discussion of theoretical uncertainties and future work.

2 BASIC EQUATIONS

The dynamical tide of the WD (mass M) is driven by the external gravitational potential of the companion (mass M'). The leading order (quadrupole) potential is

$$U_{\text{ex}}(\mathbf{r}, t) = U(r) \left[Y_{22}(\theta, \phi) e^{-i\omega t} + Y_{22}^*(\theta, \phi) e^{i\omega t} \right] \quad (1)$$

with

$$U(r) = -\frac{GM'W_{22}}{a^3} r^2. \quad (2)$$

Here a is the orbital separation, $\omega = 2\Omega$ is the tidal frequency for a non-spinning WD (we will account for the spin effect in Section 8), Ω is the orbital frequency, and $W_{22} = \sqrt{3\pi/10}$. The actual fluid perturbations in the WD can be written as $\xi_{\text{ac}}(\mathbf{r}, t) = \xi(\mathbf{r}, t) + \xi^*(\mathbf{r}, t)$ for the Lagrangian displacement and $\delta P_{\text{ac}}(\mathbf{r}, t) = \delta P(\mathbf{r}, t) + \delta P^*(\mathbf{r}, t)$ for the Eulerian pressure perturbation, and similarly for other quantities. In the following, we shall consider perturbations (ξ , δP , etc.) driven by the potential $U(\mathbf{r}, t) = U(r)Y_{22}(\theta, \phi)e^{-i\omega t}$. We shall adopt the Cowling approximation (so that the gravitational potential perturbation $\delta\Phi$ associated with the density perturbation is neglected, i.e., $\delta\Phi = 0$), which is valid for

gravity waves in the star. We will consider adiabatic oscillations, for which the Lagrangian perturbations in pressure and density are related by $\Delta P = a_s^2 \Delta \rho$, where a_s is the adiabatic sound speed. This is a good approximation in the bulk of the star where the thermal time is much longer than the wave period.

Letting

$$\delta P(\mathbf{r}, t) = \delta P(r) Y_{22}(\theta, \phi) e^{-i\omega t}, \quad (3)$$

and

$$\boldsymbol{\xi}(\mathbf{r}, t) = [\xi_r(r) \hat{r} + \xi_\perp(r) r \nabla_\perp] Y_{22}(\theta, \phi) e^{-i\omega t}, \quad (4)$$

the fluid perturbation equations reduce to

$$\frac{1}{r^2} (r^2 \xi_r)' - \frac{g}{a_s^2} \xi_r + \frac{1}{\rho a_s^2} \left(1 - \frac{L_l^2}{\omega^2}\right) \delta P - \frac{l(l+1)U}{\omega^2 r^2} = 0, \quad (5)$$

and

$$\frac{1}{\rho} \delta P' + \frac{g}{\rho a_s^2} \delta P + (N^2 - \omega^2) \xi_r + U' = 0, \quad (6)$$

where the $'$ denotes d/dr . In equations (5) and (6), L_l and N are the Lamb and Brünt-Vaisälä frequencies, respectively, given by [note we will continue to use the notations L_l , $l(l+1)$, and m , although we focus on $l = m = 2$ in this paper]

$$L_l^2 = \frac{l(l+1)a_s^2}{r^2} \quad (7)$$

and

$$N^2 = g^2 \left(\frac{d\rho}{dP} - \frac{1}{a_s^2} \right). \quad (8)$$

The other perturbation variables are related to δP and ξ_r by

$$\xi_\perp = \frac{1}{r\omega^2} \left(\frac{\delta P}{\rho} + U \right), \quad (9)$$

$$\delta \rho = \frac{1}{a_s^2} \delta P + \frac{\rho N^2}{g} \xi_r. \quad (10)$$

Defining $Z = \chi^{-1/2} r^2 \xi_r$, where

$$\chi = \frac{r^2}{\rho a_s^2} \left(\frac{L_l^2}{\omega^2} - 1 \right), \quad (11)$$

equations (5) and (6) can be combined to yield

$$Z'' + k^2(r)Z = V(r). \quad (12)$$

Here,

$$k^2(r) = \frac{\chi \rho (N^2 - \omega^2)}{r^2} + \frac{1}{2} \left(\frac{\chi'}{\chi} \right)' - \frac{1}{4} \left(\frac{\chi'}{\chi} \right)^2 + \frac{g}{a_s^2} \left[\frac{-(g/a_s^2)'}{g/a_s^2} + \frac{\chi'}{\chi} - \frac{g}{a_s^2} \right] \quad (13)$$

and

$$V(r) = \chi^{-1/2} \left[\frac{l(l+1)}{\omega^2} \left(\frac{-\chi'}{\chi} + \frac{g}{a_s^2} \right) + \frac{2r}{a_s^2} \right] U. \quad (14)$$

In the WKB limit $|k| \gg 1/H$ and $|k| \gg 1/r$, where $H = |P/P'| \simeq a_s^2/g$ is the pressure scale height, equation (13) simplifies to

$$k^2(r) = \frac{1}{a_s^2 \omega^2} (L_l^2 - \omega^2) (N^2 - \omega^2). \quad (15)$$

This is the standard WKB dispersion relation for non-radial stellar oscillations (e.g., Unno et al. 1989). For $\omega^2 \ll L_l^2$ and $\omega^2 \ll N^2$, the wave equation (12) reduces to

$$Z'' + \frac{l(l+1)(N^2 - \omega^2)}{r^2 \omega^2} Z \simeq -\chi^{-1/2} \frac{l(l+1)N^2}{\omega^2} \frac{U}{g}. \quad (16)$$

Then, as long as $|Z''/Z| \gg |\chi''/\chi|$ (which we expect to be true because $Z'' \approx -k^2 Z$ and $\chi'' \sim \chi/H^2$), equation (16) is identical to the oscillation equations used by Zahn (1975) and Goodman & Dickson (1998).

3 BOUNDARY CONDITIONS

Equations (5) and (6) or equation (12) can be solved with the appropriate boundary conditions at $r = r_{\text{out}}$ near the stellar surface and at $r = r_{\text{in}} \rightarrow 0$ at the center of the star. The general solution of equation (12) can be written as

$$Z(r) = c_+ Z_+(r) + c_- Z_-(r) + Z^{\text{eq}}(r), \quad (17)$$

where c_+ , c_- are constants. $Z_+(r)$ and $Z_-(r)$ are two independent solutions of the homogeneous equation $Z'' + k^2 Z = 0$, and $Z^{\text{eq}}(r)$ represents a particular solution of equation (12). We choose the outer boundary r_{out} to be in the wave zone ($k^2 > 0$). If $k^2(r)$ varies slowly such that $|k'/k| \ll k > 0$, then the two independent WKB solutions to the homogeneous equation are

$$Z_\pm(r) = \frac{1}{\sqrt{k}} \exp\left(\pm i \int_{r_o}^r k dr\right), \quad (18)$$

where r_o is an interior point ($r_o < r_{\text{out}}$). For $\omega^2 \ll L_l^2$, the WKB wave dispersion relation [equation (15)] reduces to $\omega^2 = N^2 k_\perp^2 / (k^2 + k_\perp^2)$, where $k_\perp^2 = l(l+1)/r^2$, which implies that the radial component of the group velocity is $-\omega k / (k^2 + k_\perp^2)$. Thus, with $\omega > 0$ and $k > 0$, $Z_- \propto e^{-i \int_{r_o}^r k dr}$ represents an outgoing wave, while $Z_+ \propto e^{i \int_{r_o}^r k dr}$ represents an ingoing wave. An approximate particular solution of equation (12) is

$$Z^{\text{eq}}(r) \simeq \frac{V}{k^2} - \frac{1}{k^2} \left(\frac{V}{k^2} \right)'' , \quad (19)$$

where the second term is smaller than the first by a factor of $(kH)^2$ or $(kr)^2$. This represents the “non-wave” equilibrium solution.¹

Throughout this paper, we adopt the radiative condition at the outer boundary ($r = r_{\text{out}}$), i.e., we require that only an outgoing wave exists:

$$Z(r) \simeq Z^{\text{eq}}(r) + \frac{c_-}{\sqrt{k}} \exp\left(-i \int_{r_o}^r k dr\right). \quad (20)$$

This implicitly assumes that waves propagating toward the WD surface are completely damped by radiative diffusion (Zahn 1975) or by non-linear processes. We will check this

¹ Note that the equilibrium tide usually refers to the f-mode response of the star to the tidal force. Here, we use the term “equilibrium” to refer to the “non-wave” solution.

assumption a posteriori from our numerical results (see Section 6.5). Thus, near the outer boundary, the radial displacement ξ_r behaves as (for $\omega^2 \ll L_l^2$)

$$\begin{aligned} \xi_r(r) &= \frac{\chi^{1/2}}{r^2} Z(r) \\ &= \xi_r^{\text{eq}}(r) + \frac{c_-}{\sqrt{\rho r^2 (N^2 - \omega^2)}} \exp\left(-i \int_{r_o}^r k dr\right). \end{aligned} \quad (21)$$

Here ξ_r^{eq} represents the equilibrium tide

$$\xi_r^{\text{eq}} \simeq \left(-\frac{U}{g}\right) \frac{N^2}{N^2 - \omega^2} \left[1 - \frac{2gr}{l(l+1)a_s^2} \frac{\omega^2}{N^2}\right], \quad (22)$$

where we have retained only the first term of equation (19). For $\omega^2 \ll N^2$, this further simplifies to $\xi_r^{\text{eq}} \simeq -U/g$ (Zahn 1975). The constant c_- specifies the amplitude of the outgoing wave which is eventually dissipated in the stellar envelope; this is the constant we wish to determine from numerical calculations.

In practice, to implement equation (21) at the outer boundary, we require a very accurate calculation of the non-wave solution ξ_r^{eq} . This can become problematic when the conditions $|k| \gg 1/H$ and $\omega \ll L_l$ are not well satisfied. Since the transverse displacement ξ_\perp for gravity waves is much larger than the radial displacement in the wave zone, it is more convenient to use ξ_\perp in our outer boundary condition. We define

$$Z_1(r) = \left(\frac{\rho}{D}\right)^{1/2} r^2 \omega^2 \xi_\perp(r), \quad (23)$$

with $D \equiv N^2 - \omega^2$. Equations (5) and (6) can be rearranged to yield

$$Z_1'' + k_1^2(r) Z_1 = V_1(r), \quad (24)$$

where

$$\begin{aligned} k_1^2(r) &= -\frac{1}{4} \left[\left(\ln \frac{\rho r^2}{D} \right)' \right]^2 - \frac{1}{2} \left(\ln \frac{\rho r^2}{D} \right)'' - \left(\frac{N^2}{g} \right)' \\ &\quad - \frac{N^2}{g} \left(\ln \frac{r^2}{D} \right)' + \frac{\omega^2}{a_s^2} + \frac{l(l+1)D}{r^2 \omega^2} \end{aligned} \quad (25)$$

and

$$\begin{aligned} V_1(r) &= -\left(\frac{\rho r^2}{D}\right)^{1/2} \times \\ &\quad \left\{ \frac{N^2}{g} U \left[\ln \left(\frac{r^2 N^2}{Dg} U \right) \right]' - \frac{\omega^2}{a_s^2} U \right\}. \end{aligned} \quad (26)$$

For $k_1 \gg 1/H$ and $\omega^2 \ll L_l^2$, the functions $k_1^2(r)$ and $V_1(r)$ simplify to

$$k_1^2(r) \simeq \frac{l(l+1)(N^2 - \omega^2)}{\omega^2 r^2} \quad (27)$$

and

$$V_1(r) \simeq -\left(\frac{\rho r^2}{D}\right)^{1/2} \frac{D}{r^2} \left(\frac{U r^2 N^2}{g D}\right)'. \quad (28)$$

Again, adopting the radiative boundary condition at $r = r_{\text{out}}$, we have

$$Z_1(r) \simeq \frac{V_1}{k_1^2} - \frac{1}{k_1^2} \left(\frac{V_1}{k_1^2}\right)'' + \frac{c_-}{k_1} \exp\left(-i \int_{r_o}^r k_1 dr\right), \quad (29)$$

where c_- is a constant. Thus, the transverse displacement $\xi_\perp(r)$ behaves as

$$\begin{aligned} \xi_\perp(r) &= \left(\frac{D}{\rho}\right)^{1/2} \frac{1}{r^2 \omega^2} Z_1(r) \\ &= \xi_\perp^{\text{eq}} + c_- \left(\frac{k_1}{\rho r^2}\right)^{1/2} \exp\left(-i \int_{r_o}^r k_1 dr\right), \end{aligned} \quad (30)$$

where several constants have been absorbed into c_- . The equilibrium tidal transverse displacement $\xi_\perp^{\text{eq}}(r)$ is given by

$$\xi_\perp^{\text{eq}}(r) \simeq -\frac{1}{l(l+1)r} \left(\frac{U r^2 N^2}{g D}\right)'. \quad (31)$$

For $\omega^2 \ll N^2$, this reduces to (for $l = 2$)

$$\xi_\perp^{\text{eq}}(r) \simeq -\frac{1}{6r} \left(\frac{U r^2}{g}\right)', \quad (32)$$

in agreement with Goldreich & Nicholson (1989). Thus, we implement the radiative boundary condition at $r = r_{\text{out}}$ as

$$\left(\xi_\perp - \xi_\perp^{\text{eq}}\right)' = \left[\frac{-\left(\rho r^2/k_1\right)'}{2\left(\rho r^2/k_1\right)} - i k_1 \right] \left(\xi_\perp - \xi_\perp^{\text{eq}}\right), \quad (33)$$

with ξ_\perp computed from ξ_r and δP using equation (9).

The inner boundary condition can be found by requiring the radial displacement to be finite at the center of the star. This requires

$$\xi_r = \frac{l}{\omega^2 r} \left(\frac{\delta P}{\rho} + U\right) \quad (\text{Near } r = 0). \quad (34)$$

4 ANGULAR MOMENTUM AND ENERGY FLUX

As the wave propagates through the star, it carries an angular momentum flux to the outer layers. At any radius within the star, the z component of the time-averaged angular momentum flux is

$$\dot{J}_z(r) = \left\langle \oint d\Omega r^2 \rho (\delta v_r + \delta v_r^*) (\delta v_\phi + \delta v_\phi^*) r \sin \theta \right\rangle, \quad (35)$$

where $\langle \dots \rangle$ implies time averaging. With

$$\delta v_r = -i\omega \xi_r(r) Y_{lm} e^{-i\omega t} \quad (36)$$

and

$$\delta v_\phi = -i\omega \xi_\perp(r) r \nabla_\phi Y_{lm} e^{-i\omega t} = \frac{m\omega \xi_\perp(r)}{\sin \theta} Y_{lm} e^{-i\omega t}, \quad (37)$$

we find

$$\begin{aligned} \dot{J}_z(r) &= 2 \oint d\Omega r^3 \rho \omega^2 \text{Re} \left[i \xi_r^*(r) Y_{lm}^* m \xi_\perp(r) Y_{lm} \right] \\ &= 2m\omega^2 \rho r^3 \text{Re} \left(i \xi_r^* \xi_\perp \right). \end{aligned} \quad (38)$$

In the wave zone, the fluid displacement consists of an equilibrium (“non-wave”) component and a dynamical (wave) component, $\xi = \xi^{\text{eq}} + \xi^{\text{dyn}}$. Since the equilibrium tide component is purely real (assuming negligible dissipation of the equilibrium tide), $\text{Re}(i \xi_r^{\text{eq}*} \xi_\perp^{\text{eq}}) = 0$, and the equilibrium tide does not contribute to angular momentum transfer. The cross terms $\text{Re}(i \xi_r^{\text{dyn}*} \xi_\perp^{\text{eq}})$, and $\text{Re}(i \xi_r^{\text{eq}*} \xi_\perp^{\text{dyn}})$ are opposed by a nearly equal and opposite Reynold’s stress

term (see Goldreich & Nicholson 1989) and do not contribute significantly to angular momentum transfer. Thus, the $\text{Re}\left(i\xi_r^{\text{dyn}*}\xi_{\perp}^{\text{dyn}}\right)$ term dominates angular momentum transfer.² Equation (38) then becomes

$$\dot{J}_z(r) = 2m\omega^2\rho r^3 \text{Re}\left[i\xi_r^{\text{dyn}*}\xi_{\perp}^{\text{dyn}}\right]. \quad (39)$$

In the outer layers of the WD where ξ^{dyn} is a pure outgoing wave ($\propto e^{-ikr}$), equation (5) can be rearranged to obtain the relationship between ξ_{\perp}^{dyn} and ξ_r^{dyn} in the WKB approximation ($k \gg 1/H$) with $\omega^2 \ll L_t^2$:

$$\xi_{\perp}^{\text{dyn}} \simeq -i\frac{kr}{l(l+1)}\xi_r^{\text{dyn}}. \quad (40)$$

Then the angular momentum flux is

$$\begin{aligned} \dot{J}_z &\simeq 2ml(l+1)\frac{\omega^2\rho r^2}{k}|\xi_{\perp}^{\text{dyn}}|^2 \\ &\simeq \frac{4\sqrt{l(l+1)}\omega^3\rho r^3}{N}|\xi_{\perp}^{\text{dyn}}|^2. \end{aligned} \quad (41)$$

where we have used the dispersion relation (equation 27) with $\omega^2 \ll N^2$ and set $m = 2$. This expression agrees with that found in Goldreich & Nicholson (1989). From the scaling of ξ_{\perp}^{dyn} provided in equation (33), we see that the angular momentum flux is constant (independent of radius) in the outer layers of the star. Since the wave pattern frequency (in the inertial frame) is Ω (the orbital frequency), the energy flux carried by the wave is given by $\dot{E} = \Omega\dot{J}_z$.

Once we have solved our differential equations (5 and 6) with the appropriate boundary conditions, we can use equation (39) to determine where angular momentum and energy are added to the wave, i.e., where the wave is generated. In the WD interior, the waves travel both inwards and outwards and thus carry no net angular momentum, so the value of \dot{J}_z oscillates around zero. However, near the outer boundary, the value of \dot{J}_z is constant and positive because there only exists an outgoing wave. The region where the value of \dot{J}_z rises to its constant value is the region of wave excitation, because it is in this region where energy and angular momentum are added to the waves (see Section 6.3).

The energy and angular momentum carried by the outgoing wave is deposited in the outer envelope of the star. Thus, the constant values of \dot{J}_z and \dot{E} near the outer boundary represent the net angular momentum and energy transfer rates from the orbit to the WD. Since $\xi_{\perp}^{\text{dyn}} \propto M'/a^3$, the angular momentum and energy transfer rates can be written in the form

$$\dot{J}_z = T_0 F(\omega), \quad \dot{E} = T_0 \Omega F(\omega), \quad (42)$$

where

$$T_0 \equiv G\left(\frac{M'}{a^3}\right)^2 R^5, \quad (43)$$

and F is a dimensionless function of the tidal frequency ω and the internal structure of the star. For WDs with rotation rate Ω_s , the tidal frequency is $\omega = 2(\Omega - \Omega_s)$.

² It can be shown that in the WKB limit the Reynold's stress associated with the dynamical response is negligible.

5 WHITE DWARF MODELS

Figure 1 depicts three WD models provided by G. Fontaine (see Brassard et al. 1991). These WD models are taken from an evolutionary sequence of a $M = 0.6M_{\odot}$ WD, at effective temperatures of $T = 10800\text{K}$, $T = 6000\text{K}$, and $T = 3300\text{K}$. The WD has a radius $R \simeq 8.97 \times 10^8\text{cm}$ and a carbon-oxygen core surrounded by a $10^{-2}M$ helium layer, which in turn is surrounded by a $10^{-4}M$ layer of hydrogen. The models shown have been slightly altered in order to ensure thermodynamic consistency (see Section 6.1).

The Brünt-Väisälä frequency can be expressed as

$$N^2 = \frac{g^2\rho}{P}\frac{\chi_T}{\chi_P}(\nabla_{\text{ad}} - \nabla + B), \quad (44)$$

where the symbols have their usual thermodynamic definitions, and the Ledoux term B accounts for composition gradients (see Brassard et al. 1991). In the core of the WD, the value of N^2 is very small due to the high degeneracy pressure, which causes χ_T in equation (44) to be small. The sharp spikes in N^2 are created by the carbon-helium and helium-hydrogen transitions, and are characteristic features of WD models. These sharp features in realistic WDs make it difficult to construct toy WD models or to understand how gravity waves propagate through the WD. From Figure 1, it is evident that cooler WDs have smaller values of N^2 throughout their interiors. However, the spikes in N^2 have little dependence on WD temperature because they are produced by composition gradients rather than thermal gradients, thus these features are unlikely to be strongly affected by tidal heating.

6 NUMERICAL CALCULATIONS OF TIDAL RESPONSE

6.1 Numerical Method and Importance of Self-Consistent Stellar Model

To calculate the amplitude of the gravity waves excited in a WD by its companion, we integrate the inhomogeneous equations (5) and (6) with the appropriate boundary conditions given by equations (33) and (34). We use the relaxation method discussed by Press et al. (2007). The integration requires a grid of points containing stellar properties (ρ , N^2 , a_s^2 , g) as a function of radius, and solves the equations on a grid of (possibly identical) relaxation points.

When creating the grid of data points representing the stellar structure, one must be very careful in ensuring that the stellar properties are consistent with one another. In particular, the Brünt Väisälä frequency is given by

$$N^2 = -g\left(\frac{\rho'}{\rho} + \frac{g}{a_s^2}\right). \quad (45)$$

If the value of N^2 in our stellar grid is not exactly equal to the right hand side of the above equation as calculated from the values of ρ , g , and a_s^2 , the stellar properties will not be self-consistent. Such inconsistency may arise from the inaccuracy of the stellar grids, or from the interpolation of the stellar grids (even if the original grids are exactly self-consistent). We have found that even a small inconsistency can lead to large error in the computed wave amplitude. The reason for this can be understood by examining equation

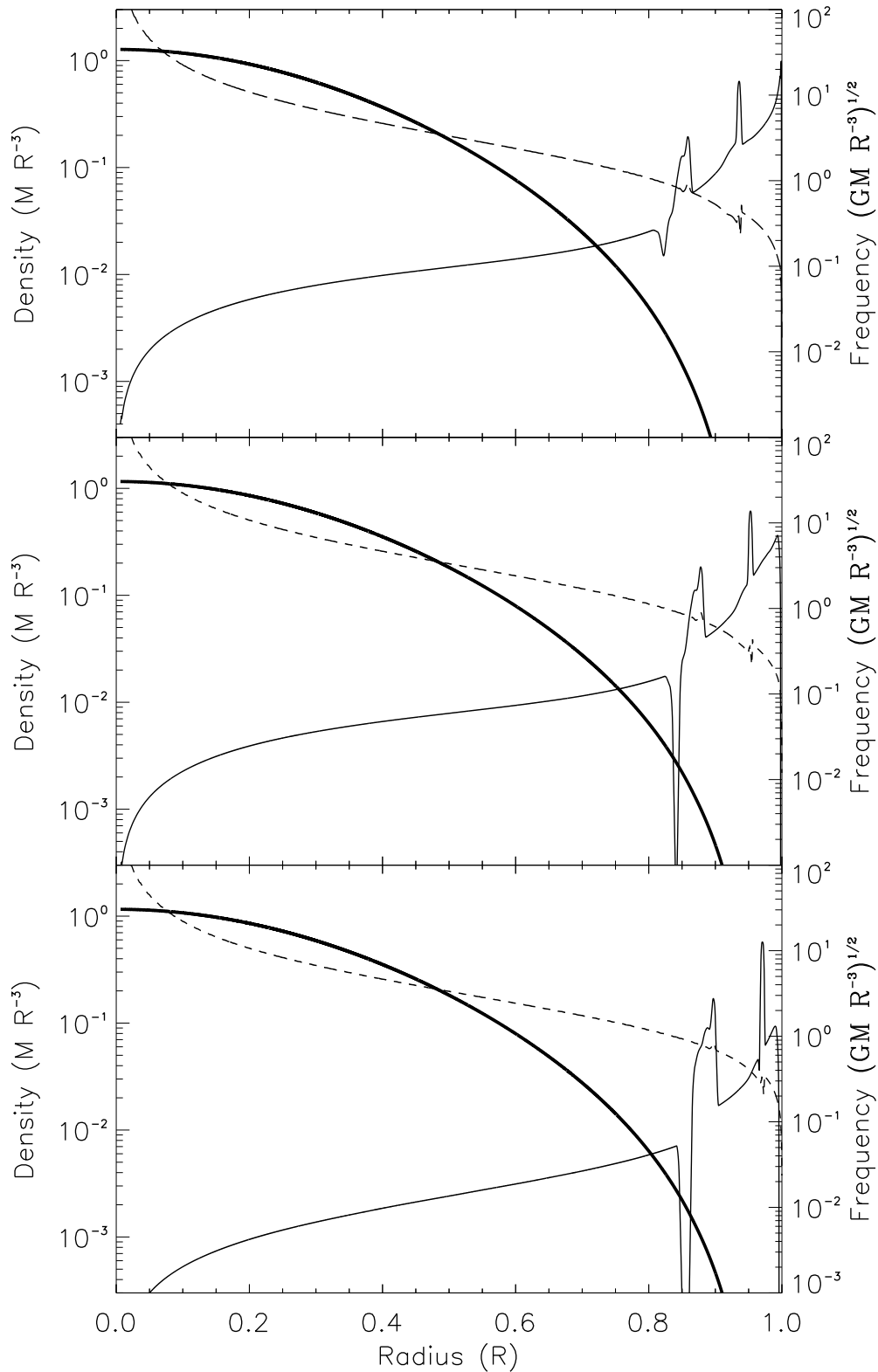


Figure 1. The square of the Brunt-Väisälä (thin solid lines) and Lamb (dashed lines) frequencies (for $l = 2$), and the density (thick solid line) as a function of normalized radius in three WD models. The models are taken from an evolutionary sequence of a DA WD with $M = 0.6M_{\odot}$, $R = 8.97 \times 10^3$ km, and effective temperatures of $T = 10800\text{K}$ (top), $T = 6000\text{K}$ (middle), and $T = 3300\text{K}$ (bottom). The spikes in the Brunt Väisälä frequency are caused by the composition changes from carbon to helium, and from helium to hydrogen, respectively. Note the formation of a convective zone just below the carbon-helium transition zone as the WD cools.

(??). When tracing back to equations (5) and (6), one can see that the N^2 term on the right-hand side is actually the sum of two terms. That is, the value of N^2 on the right-hand side of equation (16) is calculated via equation (45) from our grid of ρ , a_s^2 , and g values, while the N^2 term on the left hand side of the equation is taken directly from our grid of N^2 values. If these two values of N^2 differ (by the amount δN^2), then a “false” excitation term will be introduced on the right-hand side of equation (16), given by

$$V_f \simeq -\frac{l(l+1)\delta N^2 U}{r^2\omega^2 g}. \quad (46)$$

This false term can vary rapidly with radius depending on the error in the stellar grid. In Section 7, we discuss how sharp changes in the excitation term can be responsible for the excitation of the dynamical component of the tidal response. Thus, the false excitation term introduced by even small numerical inconsistencies can cause large errors in calculations of the dynamical tide.

To test our methods, we calculated the tidal response for a simple massive star model. The results are discussed in Appendix A, and are consistent with previous studies of gravity waves in massive stars (e.g., Zahn 1975, 1977 and Goldreich & Nicholson 1989).

6.2 Calculation with Toy White Dwarf Model

To understand wave excitation in WDs, we first examine a toy model constructed to mimic the structure of a WD. Examining the $T_{\text{eff}} = 10800\text{K}$ model, we see that it contains a sharp rise in N^2 at the carbon-helium boundary, preceded by a small dip in N^2 near the top of the carbon layer. Consequently, we have created a toy model with a similar dip and rise in N^2 in the outer part of the star. To create this model, we first construct a smooth density profile (identical to that of an $n = 2$ polytrope, along with a smooth N^2 profile that mimics the dip-rise features associated with the C-He transition in real WDs. Next, we compute a thermodynamically consistent sound speed profile using the equation

$$a_s^2 = \left(\frac{1}{dP/d\rho} - \frac{N^2}{g^2} \right)^{-1}. \quad (47)$$

Since the density profile is that of a polytrope, the $dP/d\rho$ term can be calculated analytically.

We solve the forced oscillation equations as a function of the tidal frequency ω . Figure 3 shows the energy flux and wave amplitude as a function of radius for a given value of ω . The small oscillations in energy flux are due to imperfect numerical calculation of the dynamical component of the wave and do not actually contribute to energy or angular momentum transfer. We see that waves are excited near the dip of N^2 (before N^2 rises to a maximum). This is similar to the location of wave excitation in real WD models (see Section 6.3). The dip in N^2 causes the wave to have a larger wavelength in this region, and so it couples to the companion star’s gravitational potential best in this region of the star. Note that although N^2 is smaller near the center of the star, no significant wave is excited there since $U \propto r^2$ is negligible.

Figure 4 shows a plot of $F(\omega)$. For this model, $F(\omega)$ is not a smooth, monotonic function of ω as it is for the massive star model studied in Appendix A. Instead, there are many jagged peaks and troughs, causing the value of

$F(\omega)$ to vary by two or three orders of magnitude over very small frequency ranges. These features are also present in the real WD models, and will be discussed further in Section 7. Our numerical results indicate that the peaks of $F(\omega)$ can be fitted by $F(\omega) \propto \omega^5$, significantly different from the massive star model.

6.3 Calculation with Realistic White Dwarf Model

We now present our numerical results for tidal excitations in realistic WD models. Using the outgoing wave outer boundary condition, we solved the oscillation equations (5) and (6) for the three WD models described in Section 6.2 (see Figure 1). Figures 5 and 6 show plots of the outgoing energy flux as a function of radius for the model with $T_{\text{eff}} = 10800\text{K}$ and tidal frequencies of $\omega = 2\Omega = 10^{-2}$ and 1.1×10^{-2} , in units of $G = M = R = 1$, respectively. The energy flux jumps to its final value near the carbon-helium transition zone. Once again, the oscillations in energy flux are due to imperfect numerical calculation of the dynamical component of the wave and do not actually contribute to energy or angular momentum transfer. In Figures 5 and 6, we have smoothed the value of the energy flux to minimize the amplitude of the unphysical oscillations. Note that although Figure 6 corresponds to a larger tidal frequency, the outgoing energy flux is about 100 times less than in Figure 5. Thus, as in our toy WD model (see Section 6.2), the tidal energy flux is not a monotonic function of tidal frequency as it is for early-type stars (see Section A).

We have calculated the dimensionless tidal torque $F(\omega) = \dot{J}_z/T_o$ [see equation (42)] as a function of ω for the three WD models depicted in Figure 1. The results are shown in Figures 7, 8, and 9. In general, $F(\omega)$ exhibits a strong and complicated dependence on ω , such that a small change in ω leads to a very large change in $F(\omega)$ (see also Figures 5-6). This dependence is largely due to “resonances” between the radial wavelength of the gravity waves and the radius of the carbon core, as discussed in Section 7. We also find that the local maxima of $F(\omega)$ can be approximately fitted by the scaling $F(\omega) \propto \omega^5$, similar to the toy WD model discussed in Section 6.2.

6.4 Relation to Tidal Overlap Integral

In an attempt to understand the erratic dependence of the tidal energy transfer rate \dot{E} on the tidal frequency ω , here we explore the possible relationship between \dot{E} and the tidal overlap integral. The energy transfer rate to the star due to tidal interactions can be written as

$$\dot{E} = -2 \text{Re} \int d^3x \rho \frac{\partial \xi(\mathbf{r}, t)}{\partial t} \cdot \nabla U^*(\mathbf{r}, t). \quad (48)$$

With $\xi(\mathbf{r}, t) = \xi(\mathbf{r})e^{-i\omega t}$ and $U(\mathbf{r}, t) = U(r)Y_{22}e^{-i\omega t}$ [see equations (1)-(2)], we have

$$\dot{E} = 2\omega \frac{GM'W_{22}}{a^3} \text{Im} \left[\int d^3x \rho \xi(\mathbf{r}) \cdot \nabla(r^2 Y_{22}^*) \right]. \quad (49)$$

We decompose the tidal response $\xi(\mathbf{r}, t)$ into the superposition of stellar oscillation modes (with each mode labeled by

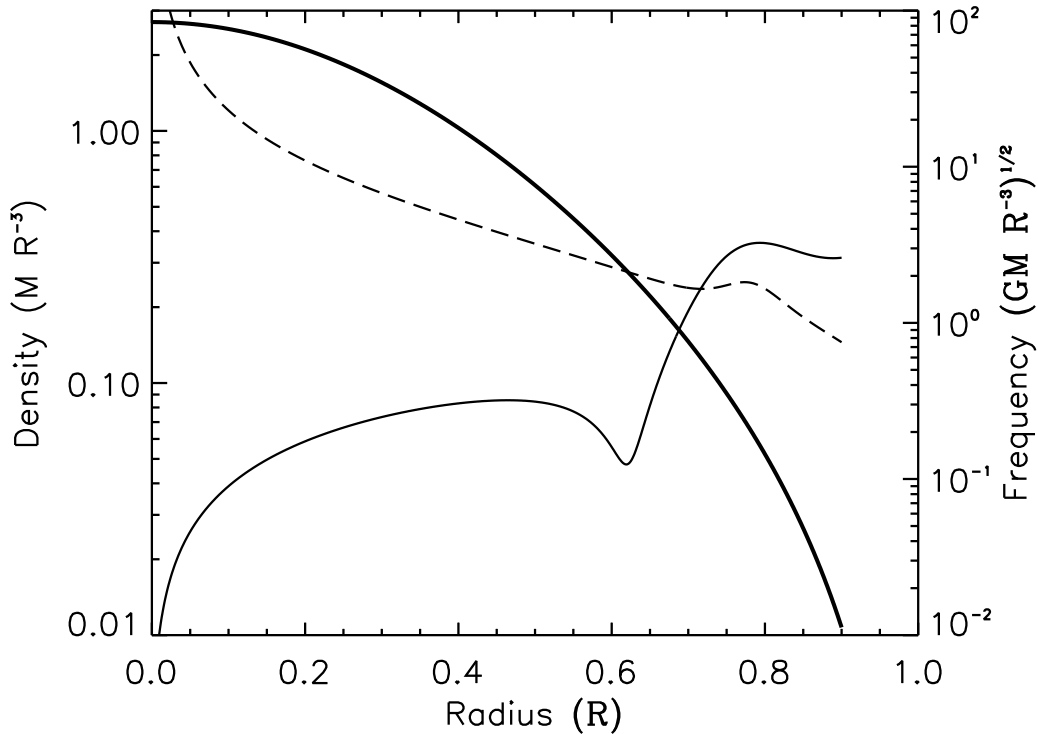


Figure 2. The square of the Brünt Vaisälä (thin solid line) and Lamb (dashed line) frequencies (for $l = 2$), in units of GM/R^3 , as a function of normalized radius in a toy WD model. Also plotted is the stellar density (thick solid line). The stellar properties are only plotted out to $r = 0.9R$, the location where the outer boundary condition is imposed in the tidal excitation calculation.

the index α):

$$\xi(\mathbf{r}, t) = \sum_{\alpha} a_{\alpha}(t) \xi_{\alpha}(\mathbf{r}), \quad (50)$$

where the mode eigenfunction ξ_{α} is normalized via $\int d^3x \rho |\xi_{\alpha}|^2 = 1$. Then the mode amplitude $a_{\alpha}(t)$ satisfies the equation

$$\ddot{a}_{\alpha} + \omega_{\alpha}^2 a_{\alpha} + \gamma_{\alpha} \dot{a}_{\alpha} = \frac{GM'W_{22}Q_{\alpha}}{a^3} e^{-i\omega t}, \quad (51)$$

where ω_{α} is the mode frequency, γ_{α} is the mode (amplitude) damping rate, and Q_{α} is the *tidal overlap integral* with mode α :

$$Q_{\alpha} = \int d^3x \rho \xi_{\alpha}^*(\mathbf{r}) \cdot \nabla(r^2 Y_{22}). \quad (52)$$

The steady-state solution of equation (51) is

$$a_{\alpha}(t) = \frac{GM'W_{22}Q_{\alpha}}{a^3(\omega_{\alpha}^2 - \omega^2 - i\gamma_{\alpha}\omega)} e^{-i\omega t}. \quad (53)$$

Thus the tidal energy transfer rate to mode α is

$$\dot{E}_{\alpha} = 2\omega \left(\frac{GM'W_{22}|Q_{\alpha}|}{a^3} \right)^2 \frac{\gamma_{\alpha}\omega}{(\omega_{\alpha}^2 - \omega^2)^2 + (\gamma_{\alpha}\omega)^2}. \quad (54)$$

In paper I, we have computed ω_{α} and Q_{α} for adiabatic g-modes of several WD models used in this paper. The eigenfunctions of these modes satisfy the “reflective” boundary condition (i.e., the Lagrangian pressure perturbation ΔP vanishes) at the WD surface. Our result showed

that although the mode frequency ω_{α} decreases as the radial mode number n increases (for a given $l = 2$), the overlap integral $|Q_{\alpha}|$ is a non-monotonic function of n (or ω_{α}) due to various features (associated with carbon-helium and helium-hydrogen transitions) in the N^2 profile of the WD models. On the other hand, our calculation of the tidal response $\xi(\mathbf{r}, t)$ presented in this paper adopts the radiative outer boundary condition; this implies significant wave damping at the outer layer of the star. Because of the difference in the outer boundary conditions, the mode frequency ω_{α} (as computed using the $\Delta P = 0$ boundary condition) does not have special significance. Nevertheless, we may expect that when $\omega = \omega_{\alpha}$, the tidal energy transfer is dominated by a single mode (α) and \dot{E} is correlated to $|Q_{\alpha}|^2$.

In Figures 7, 8, and 9 we show $|Q_{\alpha}|$ as a function of ω_{α} for a number of low-order g-modes. It is clear that the peaks and troughs of $F(\omega)$ calculated with an outgoing wave outer boundary condition are associated with the peaks and troughs in the value of $|Q_{\alpha}|^2$. Thus, the peaks in the value of $F(\omega)$ are *not* due to resonances with g-modes, but approximately correspond to the tidal frequencies near the “intrinsic frequencies” of the g-modes with large values of $|Q_{\alpha}|^2$. Note this correspondence between $|Q_{\alpha}|^2$ and the local peaks of $F(\omega)$ is not precise (as they are calculated using different boundary conditions), as is clear from the $T_{\text{eff}} = 3300\text{K}$ model (Figure 9). Another way to understand the erratic dependence of $F(\omega)$ on ω lies in the quasi-resonance cavity of the carbon core of the WD (see Section 7).

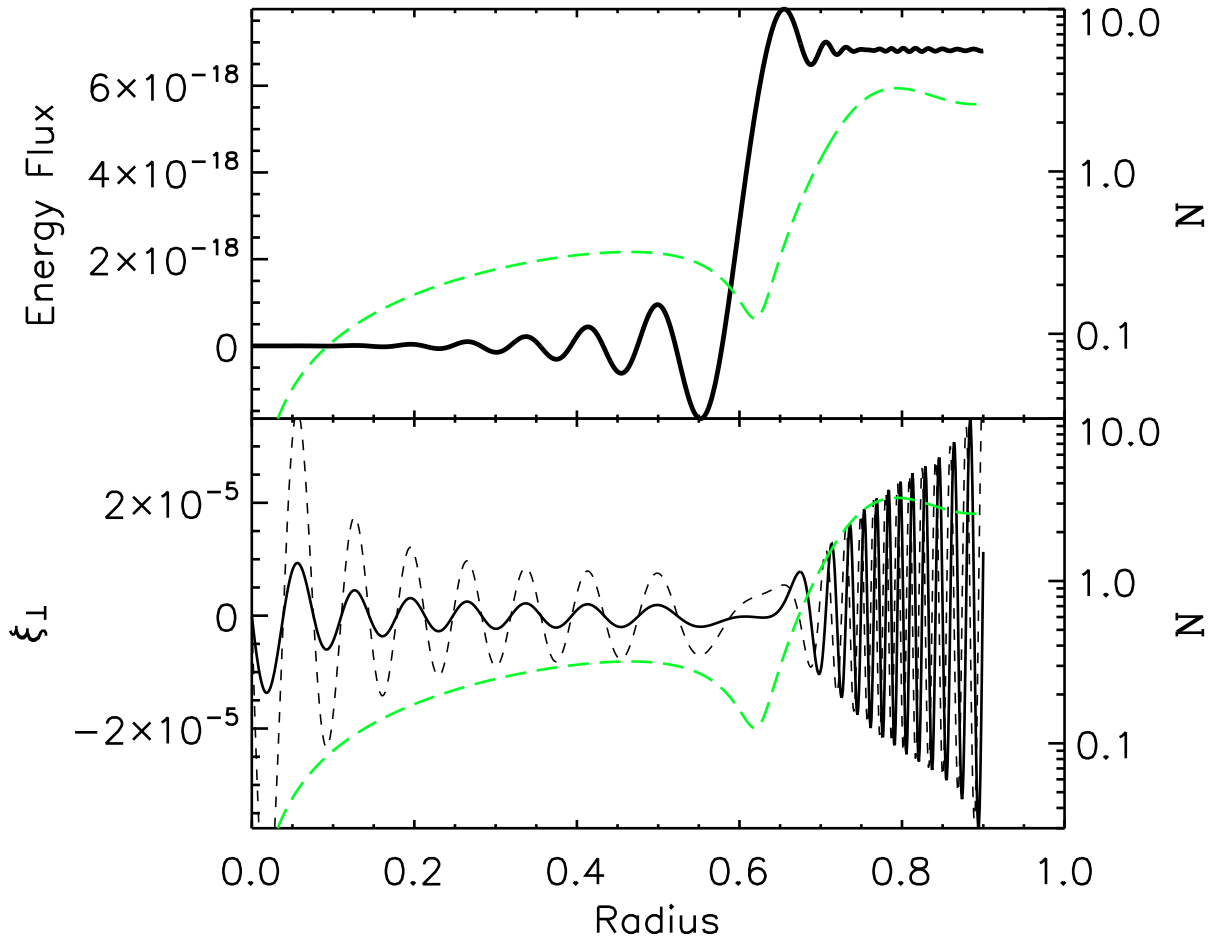


Figure 3. Dynamical tide in a toy WD model (based on the model depicted in Figure 2) driven by a companion of mass $M' = M$, with the tidal frequency $\omega = 2.3 \times 10^{-2}$. Top: The energy flux $\dot{E} = \Omega \dot{J}_z$ (dark solid line) as a function of radius, with \dot{J}_z calculated from equation (39). All values are plotted in units of $G = M = R = 1$. Bottom: The real part of ξ_{\perp}^{dyn} (dark solid line) and imaginary part of ξ_{\perp}^{dyn} (dashed line) as a function of stellar radius. The value of N^2 has been plotted (light solid green line) in both panels. In this model, the energy flux rises to its final value near the dip in N^2 , showing that the wave is excited at this location.

6.5 Justification of the Outer Boundary Condition

Our calculations in this paper adopt the outgoing wave boundary condition near the stellar surface. This implicitly assumes that gravity waves are absorbed in the outer layer of the WD due to nonlinear effects and/or radiative damping. To analyze the validity of this assumption, we plot the magnitude of the displacement, $|\xi^{\text{dyn}}|$, as a function of radius in Figure 10. We have shown the results for tidal frequencies of $\omega = 2\Omega = 0.028$ and 0.0053 (corresponding to frequencies near the peaks in $F(\omega)$ shown in Figure 7) for our WD model with $T_{\text{eff}} = 10800\text{K}$. We have also plotted the local radial wavelength k_r^{-1} because we expect nonlinear wave breaking to occur when $|\xi^{\text{dyn}}| \gtrsim k_r^{-1}$.

It is evident from Figure 10 that at relatively high tidal frequencies, the gravity waves become nonlinear in the outer layer of the star, justifying our outgoing wave boundary condition. In some cases, the waves formally reach nonlinear amplitudes ($k_r^{-1}|\xi^{\text{dyn}}| > 1$) in the helium-hydrogen transition region (demarcated by the dip in k_r^{-1} at $r \simeq 0.935$). This implies that waves may be partially reflected at the helium-hydrogen transition region, although nonlinear damping

may also occur before the waves make it to the outermost layers of the WD. The lower frequency gravity waves do not formally reach nonlinear amplitudes in the region depicted in Figure 10. However, when extending to the lower-density region near the stellar surface, the wave amplitudes will increase further and nonlinearity will set in, although partial reflection may occur due to the shallow convection zone very near the stellar surface. Also note that our calculations are for $\Omega_s = 0$. If the WD has a non-negligible spin (Ω_s), a given tidal frequency $\omega = 2(\Omega - \Omega_s)$ would correspond to a higher orbital frequency Ω , further increasing the wave amplitudes compared to those shown in Figure 10. Furthermore, lower frequency waves may damp efficiently via radiative diffusion near the stellar surface. We therefore expect our outgoing wave outer boundary condition to be a good approximation for the frequencies considered in this paper for our warmest WD model.

Our cooler WD models with $T_{\text{eff}} = 6000\text{K}$ and $T_{\text{eff}} = 3300\text{K}$ do not formally reach the same nonlinear amplitudes as our warmest model. The cooler models have smaller Brunt-Vaisala frequencies, particularly in their outer layers, as can be seen in Figure 1. Consequently, the gravity

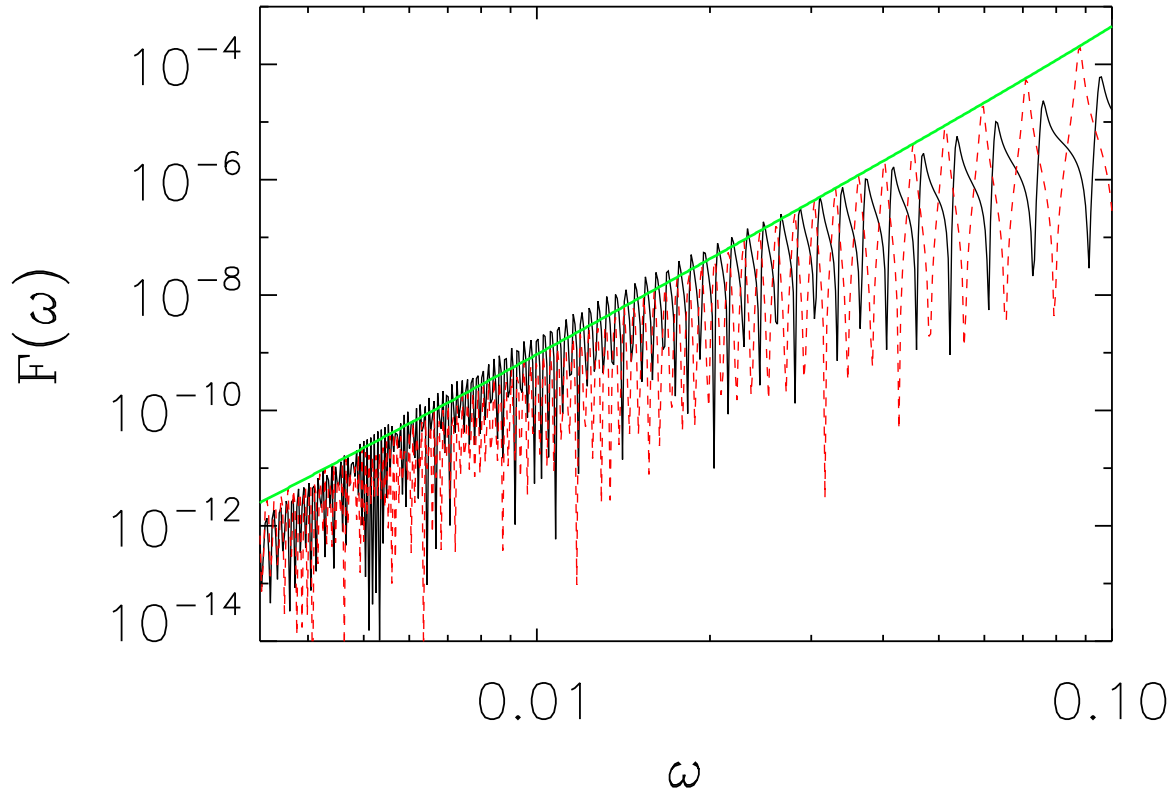


Figure 4. The dimensionless tidal torque $F(\omega) = \dot{J}_z/T_o$ [see equation (42)] carried by the outgoing gravity wave as a function of the tidal frequency ω (solid line), for the toy WD model depicted in Figure 2. The frequency is in units of $G = M = R = 1$. The straight light solid (green) line is calculated from equation (68) and is roughly proportional to ω^5 . The dashed (red) line is our semi-analytical approximation, with $\alpha = 1/5$, $\beta = 1/5$, and $\delta = 0$ (see Section 7).

waves have smaller displacements (recall the WKB scaling $\xi_{\perp}^{\text{dyn}} \propto N^{1/2}$ for a constant \dot{J}_z) and larger wavelengths (recall $k_r \propto N$). Therefore, gravity waves are less likely to damp due to nonlinear effects in our cooler models, and our outgoing wave outer boundary condition may not be justified at all frequencies considered. More detailed analyses of the nonlinear effects in dynamical tides are necessary (e.g., Barker & Ogilvie 2010, Weinberg et al. 2011).

7 SIMPLE MODEL FOR GRAVITY WAVE EXCITATION: ANALYTICAL ESTIMATE

To understand our numerical result for the tidal energy transfer rate \dot{E} (Section 6.3), particularly its dependence on the tidal frequency ω , here we consider a simple stellar model that, we believe, captures the essential physics of tidal excitation of gravity waves in binary WDs. In this model, the star consists of two regions (see Figure 11): the outer region with $r > r_a$ (region a) and the inner region with $r < r_b$ (region b). In each region, the stellar profiles are smooth, but N^2 jumps from N_b^2 at $r = r_b$ to N_a^2 (with $N_a^2 \gg N_b^2$) at $r = r_a$. The tidal frequency ω satisfies $\omega^2 \ll N_b^2$. As we will see, although waves can propagate in both regions, the sharp jump in N^2 makes the inner region behave like a resonance cavity—this is ultimately responsible for the erratic dependence of $F(\omega)$ on the tidal frequency ω .

We start from the wave equation (12) for $Z(r) =$

$\chi^{-1/2} r^2 \xi_r$:

$$Z'' + k^2(r)Z = V(r), \quad (55)$$

with

$$\begin{aligned} k^2(r) &= \frac{l(l+1)N^2}{r^2\omega^2} + \Delta k^2(r) \\ &= \frac{l(l+1)N^2}{r^2\omega^2} \left\{ 1 + \mathcal{O}\left[\frac{r^2}{H^2} \frac{\omega^2}{l(l+1)N^2}\right] \right\} \end{aligned} \quad (56)$$

$$V(r) = -\chi^{-1/2} \frac{l(l+1)N^2}{\omega^2} \frac{U}{g} \left[1 - \frac{2r}{H} \frac{\omega^2}{l(l+1)N^2} \right], \quad (57)$$

where $H = a_s^2/g (\lesssim r)$ is the pressure scale height. The above expressions are valid in both regions of the star, and we have assumed $\omega^2 \ll L_i^2$ and $\omega^2 \ll N^2$ [more general expressions are given by equations (13) and (14)]. Since the stellar profiles are smooth in each of the two regions, the non-wave (“equilibrium”) solution is given by

$$Z^{\text{eq}}(r) \simeq \frac{V}{k^2} - \frac{1}{k^2} \left(\frac{V}{k^2} \right)'' = Z_0 + \Delta Z, \quad (58)$$

where

$$Z_0 = -\chi^{-1/2} \frac{r^2 U}{g}, \quad (59)$$

$$\Delta Z = Z_0 \frac{\beta}{k^2 H^2}, \quad (60)$$

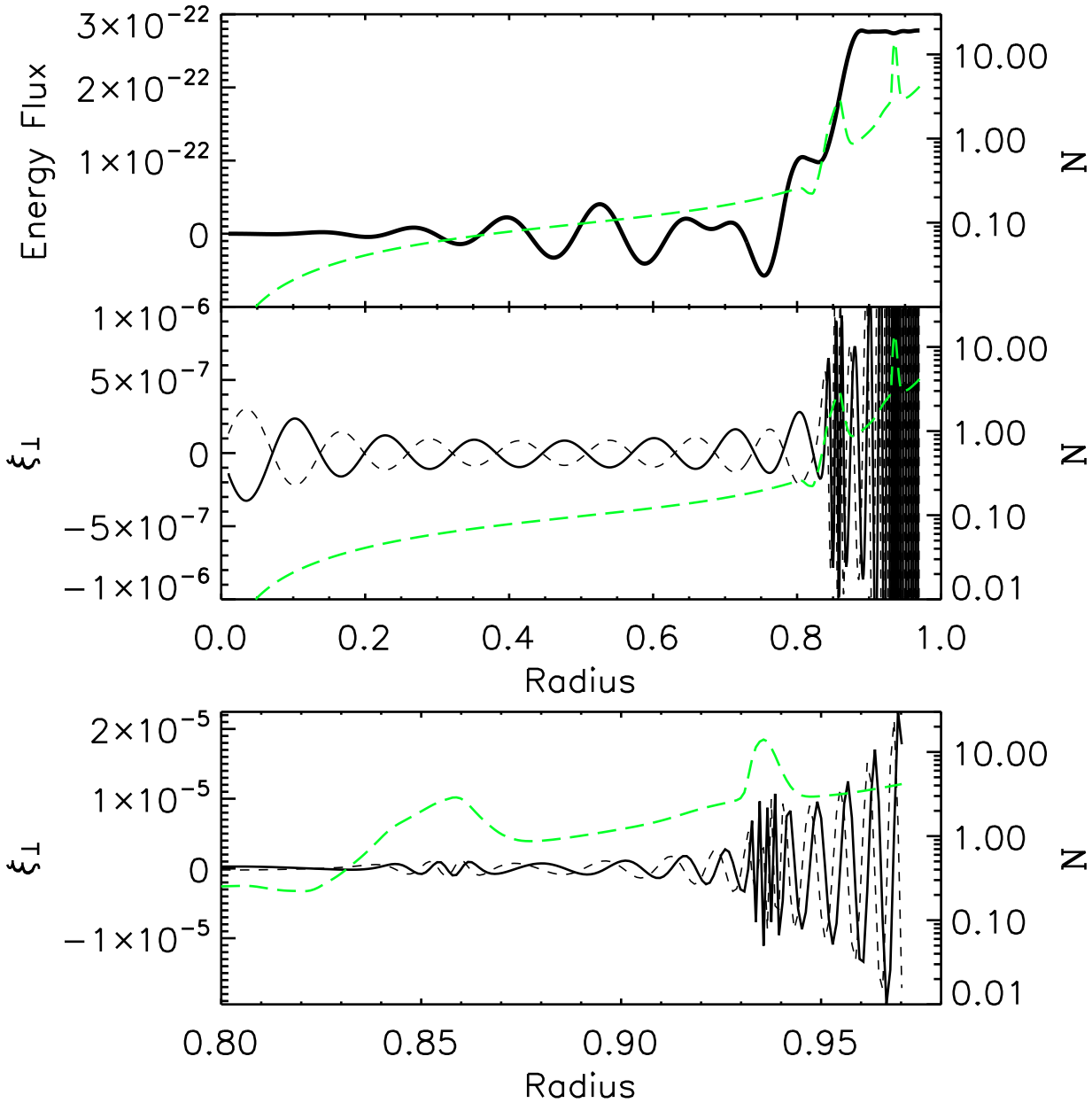


Figure 5. Dynamical tide in a realistic WD model (with $M = 0.6M_{\odot}$, $R = 8.97 \times 10^3 \text{ km}$, and $T_{\text{eff}} = 10800 \text{ K}$) driven by a companion of mass $M' = M$, with the tidal frequency $\omega = 2\Omega = 10^{-2}$. Top: The energy flux $\dot{E} = \Omega \dot{J}_z$ (thick solid line) as a function of radius, calculated from equation (39). All values are plotted in units of $G = M = R = 1$. Middle: The real part of ξ_{\perp}^{dyn} (solid line) and imaginary part of ξ_{\perp}^{dyn} (dashed line) as a function of stellar radius. Bottom: The same as the middle panel, but zoomed in on the outer layer of the WD. The value of N^2 has been plotted as dashed (green) lines in each panel. The energy flux rises to near its final value around the carbon-helium transition region, showing that the wave is excited at this location.

and β is a constant (with $\beta \sim 1$).³ Note that the above solution for Z^{eq} breaks down around $r = r_{\text{in}}$ (where $\omega^2 =$

N^2). At distances sufficiently far away from r_{in} , we have $k \gg 1/H$.

The general solution to equation (12) consists of the non-wave part Z^{eq} and the wave part Z^{dyn} . In region b there exist both ingoing and outgoing waves. Thus

$$Z(r) = Z^{\text{eq}}(r) + A_+ \exp\left(i \int_{r_{\text{in}}}^r k dr\right) + A_- \exp\left(-i \int_{r_{\text{in}}}^r k dr\right) \quad (61)$$

³ From equation (13), we find that Δk^2 in equation (56) is given by $\Delta k^2 = (H_{\rho}^{-1})'/2 - (2H_{\rho})^{-2} + H_p^{-1}[-(\ln H_p)' + H_{\rho}^{-1} - H_p^{-1}]$, where $H_p = H$ and $H_{\rho} = -\rho'/\rho$. In the isothermal region, $H_{\rho} = H$, and we have $\Delta k^2 = -(2H_{\rho})^{-2}$. In the region satisfying $P \propto \rho^{5/3}$, we have $H_{\rho} = (5/3)H$, and $\Delta k^2 \simeq 1/(12H_{\rho}^2)$. Thus the parameter β in equation (59) ranges from $|\beta| \lesssim 0.1$ to 0.3.

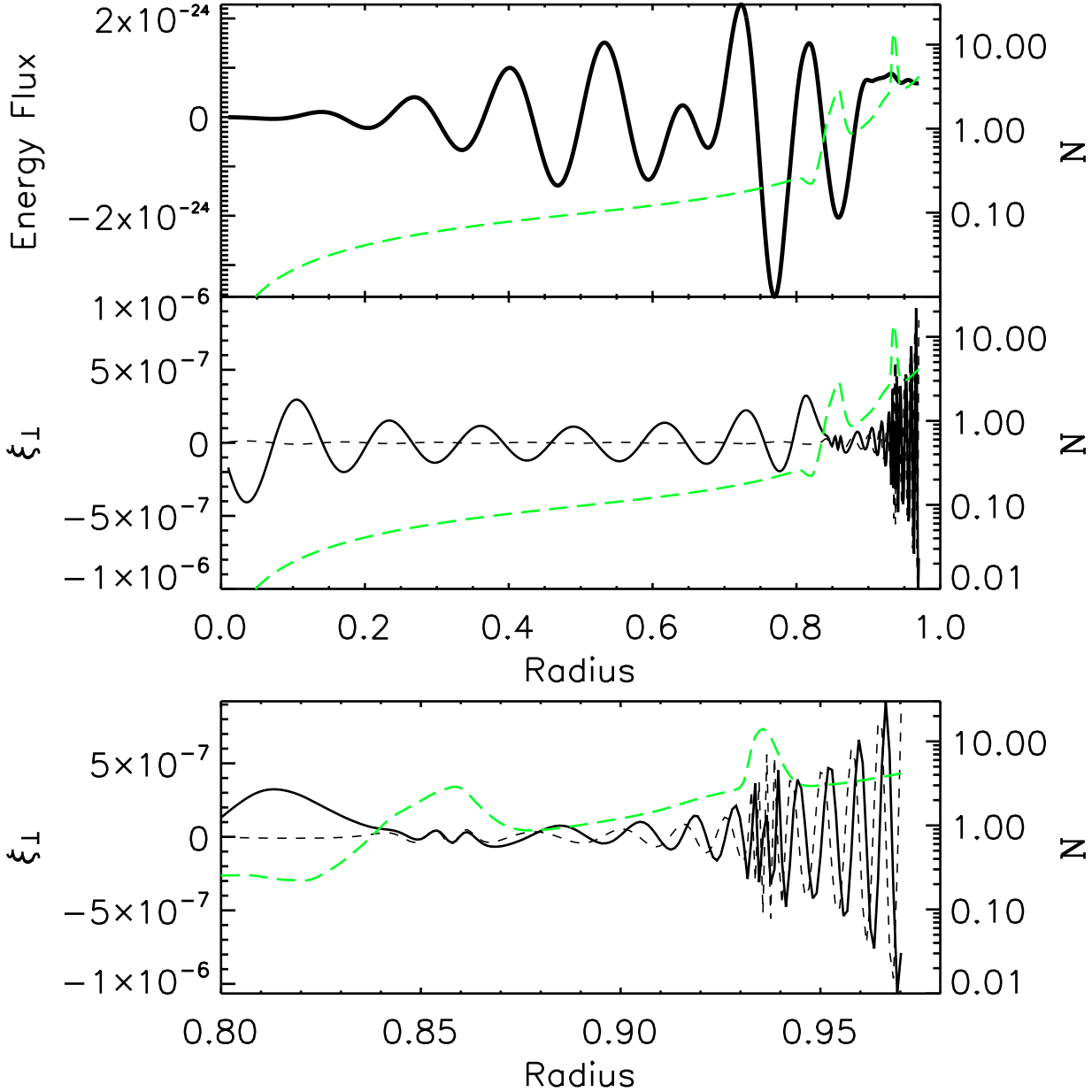


Figure 6. Same as Figure 5, but for the tidal frequency $\omega = 1.1 \times 10^{-2}$.

for $r_{\text{in}} < r < r_b$, where A_+ and A_- are slow-varying functions of r . In region a, we require there be no ingoing wave. Thus for $r > r_a$,

$$Z(r) = Z^{\text{eq}}(r) + A \exp\left(-i \int_{r_0}^r k dr\right) \quad (62)$$

where $r_0 > r_a$ is a constant, and A varies slowly with r . Note that Z^{eq} is discontinuous between the two regions.

At the inner boundary $r = r_{\text{in}}$, gravity waves are perfectly reflected. Thus we have $A_- = -e^{i\delta} A_+$, where δ is a constant phase that depends on the details of the disturbance around and inside r_{in} . To determine A and A_+ we must match the solutions in the two regions. Although in reality r_a is somewhat larger than r_b , we shall make the approximation $r_a \simeq r_b$, and label the physical quan-

tities on each side with the subscript ‘‘a’’ or ‘‘b’’. Note that $Z_a^{\text{eq}} - Z_b^{\text{eq}} \simeq -\Delta Z_b$ since $k_a^2 \gg k_b^2$, and $(dZ^{\text{eq}}/dr)_a - (dZ^{\text{eq}}/dr)_b \simeq -(\alpha/H)\Delta Z_b$ where α is a constant ($|\alpha| \sim 1$). Matching Z and dZ/dr across $r = r_b \simeq r_a$, we obtain the expression for the wave amplitude at $r = r_a$:

$$A \exp\left(-i \int_{r_0}^{r_a} k dr\right) = \Delta Z_b \left[\frac{1 - (\alpha/k_b H) \tan \varphi}{1 + i(k_a/k_b) \tan \varphi} \right], \quad (63)$$

which entails

$$|A| = |\Delta Z_b| \frac{|1 - (\alpha/k_b H) \tan \varphi|}{[1 + (k_a/k_b)^2 \tan^2 \varphi]^{1/2}}, \quad (64)$$

where

$$\varphi = \int_{r_0}^{r_b} k dr - \frac{\delta}{2}. \quad (65)$$

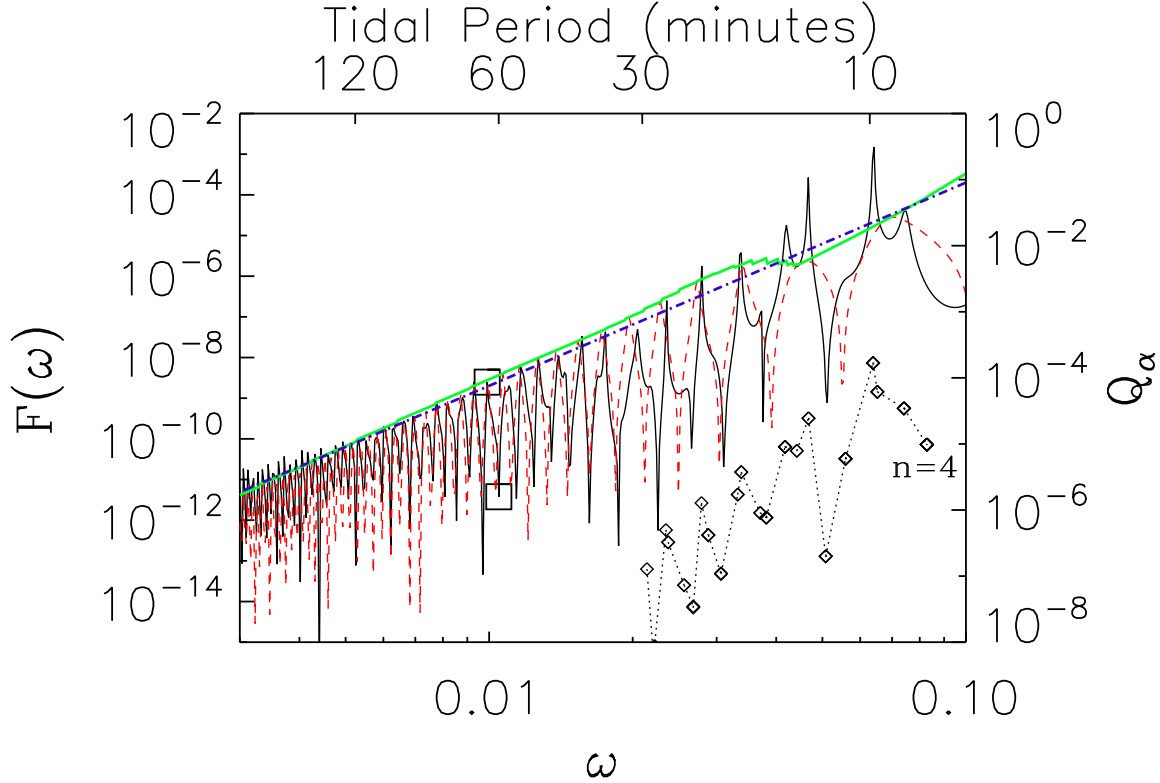


Figure 7. The dimensionless tidal torque $F(\omega) = \dot{J}_z/T_o$ [see equation (42)] carried by outgoing gravity waves as a function of the tidal frequency ω for our WD model with $T_{\text{eff}} = 10800\text{K}$. The two boxed points correspond to $\omega = 10^{-2}$ and 1.1×10^{-2} , as depicted in Figures 5 and 6. The dashed (red) line is our semi-analytical approximation [see equation (67)], with $\alpha = 1/5$, $\beta = 1/5$, and $\delta = 0$. The smooth solid line corresponds to the maximum values of $F(\omega)$ in our semi-analytical equation, and is calculated from equation (69). The dot-dashed (blue) line corresponds to $F(\omega) = 20\omega^5$ (see Section 8). The diamonds connected by the dotted line are the tidal overlap integrals Q_α associated with nearby gravity modes, and the $n = 4$ mode is the highest frequency mode shown. The frequency and Q_α are plotted in units of $G = M = R = 1$.

Clearly, $|A|$ reaches the maximum $|\Delta Z_b|$ at $\varphi = 0$, and $|A| \simeq |\Delta Z_b(\alpha/k_a H)|$ at $\varphi = \pi/2$.

The Lagrangian displacement for the outgoing gravity wave in region a is given by

$$\begin{aligned} \xi_\perp^{\text{dyn}} &\simeq -\frac{ikr}{l(l+1)}\xi_r^{\text{dyn}} \\ &= -\frac{ik\chi^{1/2}}{l(l+1)r}A \exp\left(-i\int_{r_0}^r k dr\right). \end{aligned} \quad (66)$$

The tidal energy transfer rate \dot{E} is equal to the energy flux carried by the wave. Using equation (41), we have

$$\dot{E} = \Omega \dot{J}_z = 4\Omega k_a |A|^2, \quad (67)$$

where $k_a = \sqrt{l(l+1)}N_a/(r_a\omega)$ and $|A|$ are evaluated at $r = r_a$. Using $|A|_{\text{max}} = |\Delta Z_b|$, we obtain the maximum tidal energy transfer rate as a function of the tidal frequency ω and the orbital frequency Ω :

$$\dot{E}_{\text{max}} \simeq \frac{6\pi\beta^2}{5} \frac{\rho_a r_a^7 N_a}{N_b^4 [l(l+1)]^{5/2} g_a^2} \left(\frac{r_a}{H_a}\right)^4 \left(\frac{M'}{M_t}\right)^2 \Omega^5 \omega^5. \quad (68)$$

The corresponding dimensionless tidal torque [see equation (42)] is

$$F_{\text{max}}(\omega) = \frac{6\pi\beta^2}{5} \frac{G\rho_a r_a^7 N_a}{N_b^4 [l(l+1)]^{5/2} g_a^2 R^5} \left(\frac{r_a}{H_a}\right)^4 \omega^5. \quad (69)$$

This scaling [$F(\omega) \propto \omega^5$] agrees with our numerical results for the toy WD models (Section 6.2) and realistic WD models (Section 6.3).

Realistic WD models are obviously more complicated than the analytical model considered in this section (see Figure 11). To evaluate the tidal energy transfer rate \dot{E} using equation (67) [with $|A|$ given by equation (64)] and \dot{E}_{max} using equation (68) for our WD models, we choose r_b at the location where $d \ln N^2 / dr$ is largest in the helium-carbon transition region. We then set the location of r_a to be one half of a wavelength above r_b , i.e., by finding the location r_a such that the equation $\pi = \int_{r_b}^{r_a} k dr$ is satisfied, where k is given by equation (27). For the three models considered in Section 6, we find that r_a thus calculated typically lies near the peak in N^2 associated with the carbon-helium transition region.

In Figures 4, 7, 8, and 9, we compare the analytical results based on equations (67) and (68) to our numerical calculations. We see that the erratic dependence of $F(\omega)$ on the tidal frequency ω can be qualitatively reproduced by our analytical expression (67), and the maximum F_{max} is also well approximated by equation (69). Our analytical estimate works best for the WD model with $T_{\text{eff}} = 10800\text{K}$, but it does a poor job of approximating the value of $F(\omega)$ for the WD model with $T_{\text{eff}} = 3300\text{K}$. We attribute this dis-

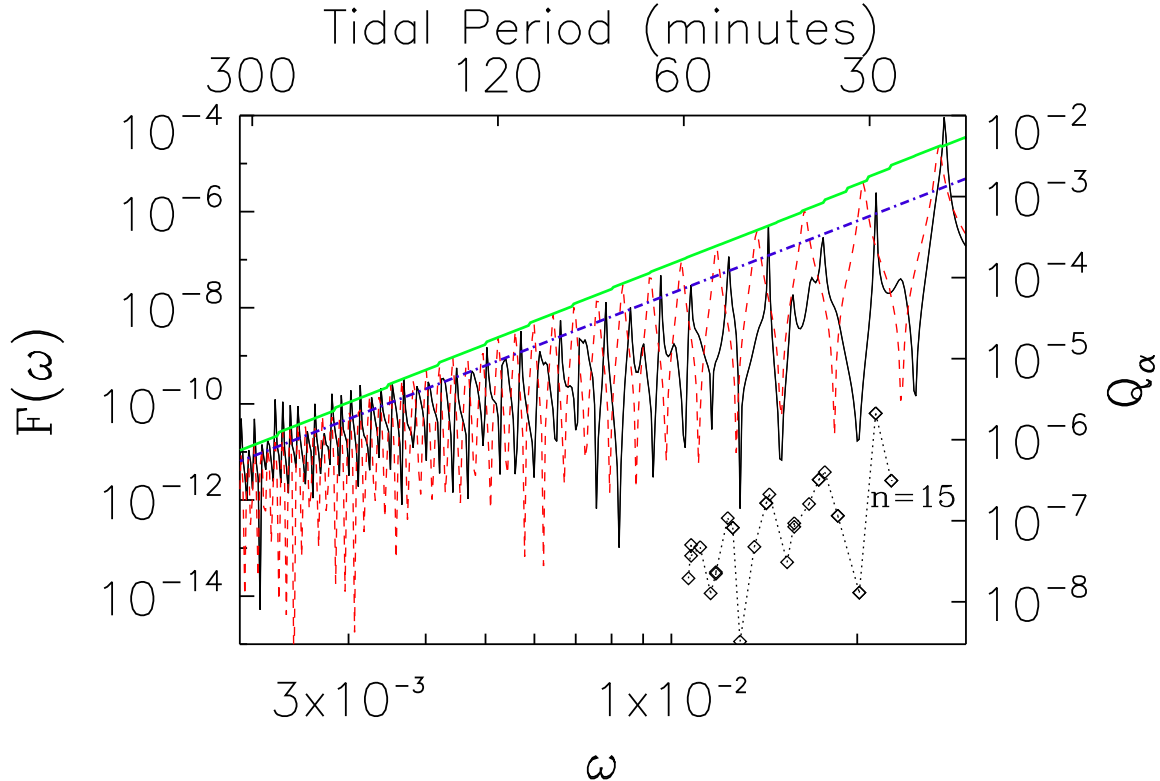


Figure 8. Same as Figure 7, except for the $T_{\text{eff}} = 6000\text{K}$ WD model. In this plot, the dot-dashed (blue) line corresponds to $F(\omega) = 200\omega^5$. The $n = 15$ mode is the highest frequency g-mode shown.

agreement to the lower value of N^2 in the cool WD model because our assumption that $N^2 \gg \omega^2$ is not satisfied. Instead, we find that gravity waves are excited near the spike in N^2 associated with the helium-hydrogen transition region in the cool WD model.

For each model shown in Figures 7-9, our model also breaks down at the highest and lowest frequencies shown. These discrepancies are likely related to errors in our numerical methods. At the highest frequencies shown, the approximation $k_r \gg 1/H$ begins to break down, causing error in our outer boundary condition. At the lowest frequencies shown, extremely fine grid resolution is needed to resolve the dynamical component of the tidal response, and so slight thermodynamic inconsistencies may introduce significant errors (see Section 6.1).

8 SPIN-ORBIT EVOLUTION

The tidally-excited gravity waves and their dissipations cause energy and angular momentum transfer from the orbit to the star, leading to spin-up of the WD over time. In this section, we study the spin-orbit evolution of WD binaries under the combined effects of tidal dissipation and gravitational radiation. In general, the tidal torque on the primary star M from the companion M' and the tidal energy transfer rate can be written as [see equations (42) and (43)]

$$T_{\text{tide}} = T_0 F(\omega), \quad \dot{E}_{\text{tide}} = T_0 \Omega F(\omega), \quad (70)$$

with $T_0 = G(M'/a^3)^2 R^5$. In previous sections, we have computed $F(\omega)$ for various non-rotating ($\Omega_s = 0$) WD models (and other stellar models). To study the spin-orbit evolution, here we assume that for spinning WDs, the function $F(\omega)$ is the same as in the non-rotating case. This is an approximation because a finite Ω_s can modify gravity waves in the star through the Coriolis force (gravity waves become the so-called Hough waves) and introduce inertial waves, which may play a role in the dynamical tides. In other words, the function F generally depends on not only ω but also Ω_s . However, we expect that when the tidal frequency $\omega = 2(\Omega - \Omega_s)$ is larger than Ω_s , i.e., when $\Omega \gtrsim 3\Omega_s/2$, the effect of rotation on the gravity waves is small or modest. Also, we assume that the WD exhibits solid-body rotation, which would occur if different layers of the WD are strongly coupled (e.g., due to viscous or magnetic stresses).⁴

Before proceeding, we note that in the weak friction theory of equilibrium tides (e.g., Darwin 1879; Goldreich & Soter 1966; Alexander 1973; Hut 1981), the tidal torque is related to the tidal lag angle δ_{lag} or the tidal lag time Δt_{lag}

⁴ In a medium containing a magnetic field, we expect differential rotation to be smoothed out by magnetic stresses on time scales comparable to the Alfvén wave crossing time. The Alfvén wave crossing time is $t_A = R\sqrt{4\pi\rho}/B \simeq 1\text{yr}$ for a magnetic field strength of $B = 10^5\text{gauss}$ and a density of $\rho = 10^6\text{g/cm}^3$. Since the Alfvén wave crossing time is always much smaller than the inspiral time for WDs, we expect solid body rotation to be a good approximation.

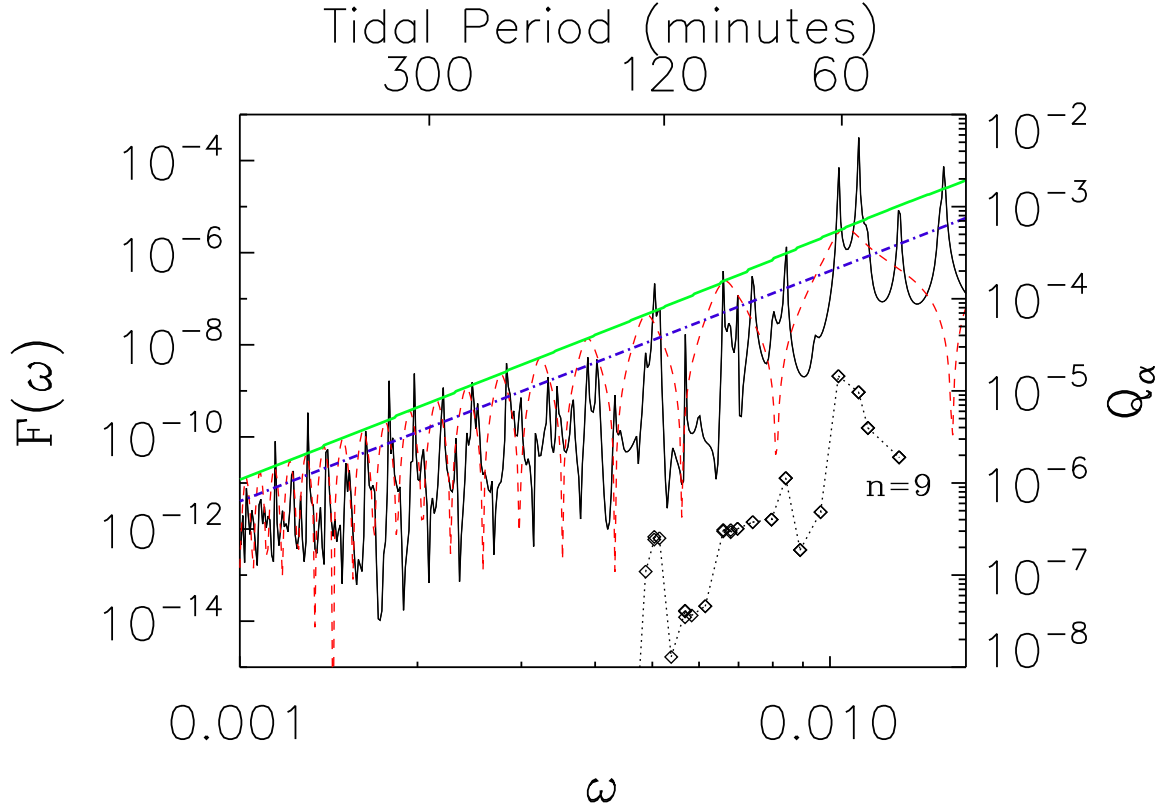


Figure 9. Same as Figure 7, except for the $T_{\text{eff}} = 3300\text{K}$ WD model. In this plot, the dot-dashed (blue) line corresponds to $F(\omega) = 4 \times 10^3 \omega^5$. The $n = 9$ mode is the highest frequency g-mode shown.

by

$$T_{\text{tide}} = 3k_2 T_0 \delta_{\text{lag}}, \quad \text{with } \delta_{\text{lag}} = (\Omega - \Omega_s) \Delta t_{\text{lag}}, \quad (71)$$

where k_2 is the Love number. Often, a dimensionless tidal quality factor Q_{tide} is introduced (e.g. Goldreich & Soter 1966) such that $\Delta t_{\text{lag}} = 1/(|\omega| Q_{\text{tide}})$ (valid only for $\omega \neq 0$). Thus, if we use the weak-friction theory to parametrize our dynamical tide, $F(\omega)$ would correspond to

$$\begin{aligned} F(\omega) &= 3k_2 \delta_{\text{lag}} \\ &= 3k_2 (\Omega - \Omega_s) \Delta t_{\text{lag}} \\ &= \frac{3k_2}{2Q_{\text{tide}}} \text{sgn}(\Omega - \Omega_s). \end{aligned} \quad (72)$$

Obviously, the effective Q_{tide} would depend strongly on ω as opposed to being a constant (assuming constant lag angle) or being proportional to $1/|\omega|$ (assuming constant lag time, appropriate for a viscous fluid).

With equation (70) and the assumption in $F(\omega)$, the WD spin evolves according to the equation

$$\dot{\Omega}_s = \frac{T_0 F(\omega)}{I}, \quad (73)$$

where I is the moment of inertia of the WD ($I \simeq 0.169MR^2$ for our $M = 0.6M_\odot$ WD models). The orbital energy $E_{\text{orb}} = -GMM'/(2a)$ satisfies the equation

$$\dot{E}_{\text{orb}} = -\dot{E}_{\text{tide}} - \dot{E}_{\text{GW}}, \quad (74)$$

where $\dot{E}_{\text{GW}} (> 0)$ is the energy loss rate due to gravitational radiation. The evolution equation for the orbital angular

frequency $\Omega = (GM_t/a^3)^{1/2}$ is then

$$\dot{\Omega} = \frac{3T_0 F(\omega)}{\mu a^2} + \frac{3\Omega}{2t_{\text{GW}}}, \quad (75)$$

where $\mu = MM'/M_t$ is the reduced mass of the binary, and t_{GW} is the orbital decay time scale ($|a/\dot{a}|$) due to gravitational radiation:

$$\begin{aligned} t_{\text{GW}} &= \frac{5c^5}{64G^3} \frac{a^4}{MM'M_t} \\ &= 3.2 \times 10^{10} \left(\frac{M_\odot^2}{MM'} \right) \left(\frac{M_t}{2M_\odot} \right)^{1/3} \left(\frac{\Omega}{0.1 \text{ s}^{-1}} \right)^{-8/3} \text{ s}, \end{aligned} \quad (76)$$

8.1 Synchronization

Using our results for the function $F(\omega)$ obtained in previous sections, we integrate equations (73) and (75) numerically to obtain the evolution of the WD spin. Since at large a (small Ω) the orbital decay time $\sim t_{\text{GW}} \propto \Omega^{-8/3}$ is much shorter than the time scale for spin evolution, $t_{\text{spin}} = \Omega_s/\dot{\Omega}_s \propto 1/(\Omega^4 F)$, we start our integration with $\Omega_s \ll \Omega$ at a small orbital frequency (an orbital period of several hours).

The results for our three WD models are shown in Figures 12 and 13. Note we only include the effects of tides in the primary star (M), and treat the companion (M') as a point mass. All three models have the same WD masses ($M = M' = 0.6M_\odot$), but different temperatures. Also note that the minimum binary separation (before mass transfer or tidal disruption occurs) is $a_{\text{min}} \simeq 2.5(M_t/M)^{1/3}R$, corre-

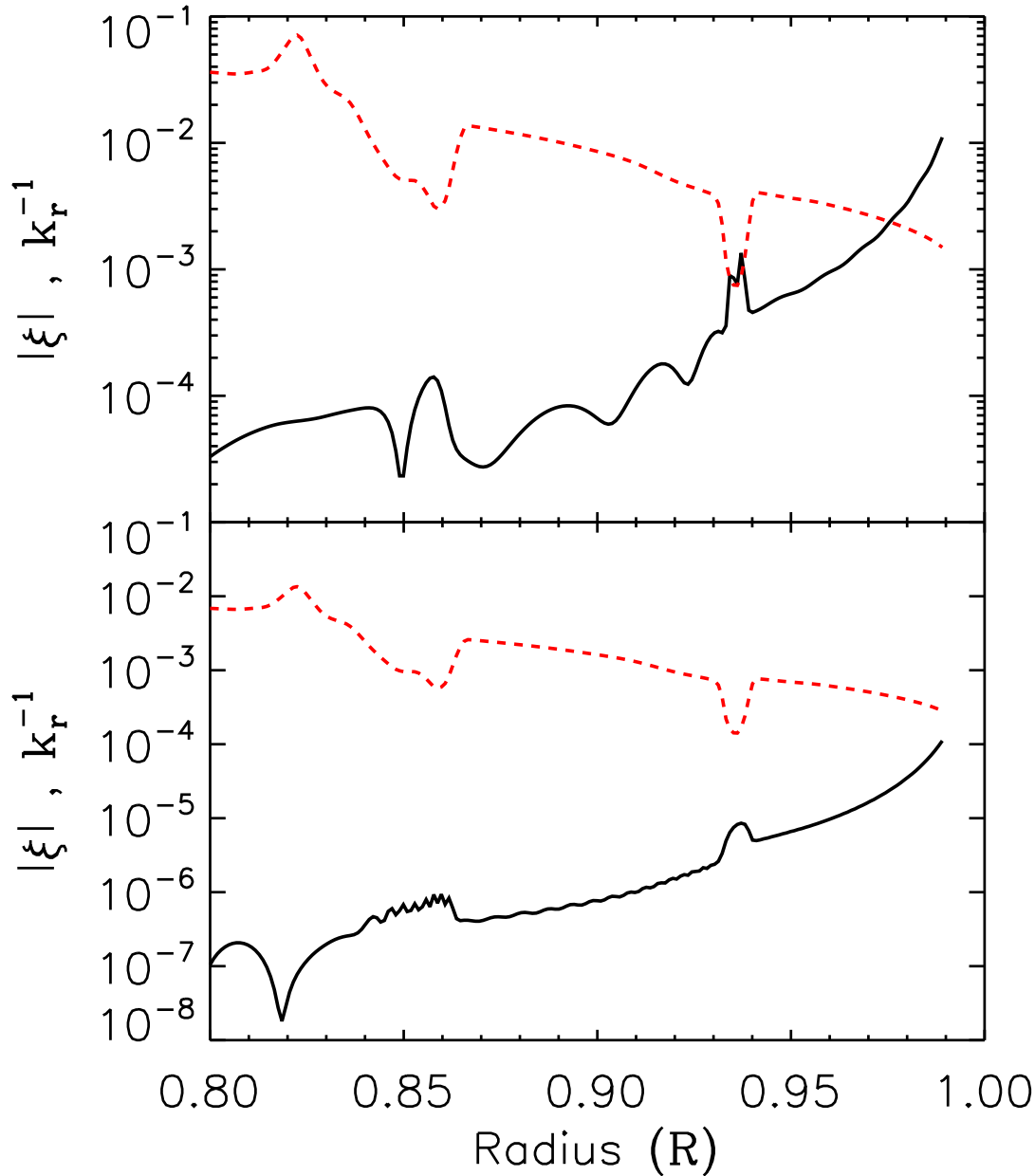


Figure 10. The magnitude of the gravity wave displacement vector $|\xi^{\text{dyn}}|$ (solid line) as a function of radius for a tidal frequency of $\omega = 0.028$ (top) and $\omega = 0.0053$ (bottom). Also plotted is the local radial wavelength k_r^{-1} (red dashed line). The wave displacement, wavelength, and frequency are in units where $G = M = R = 1$.

sponding to the minimum orbital period

$$P_{\text{min}} \simeq (1.1 \text{ min}) M_1^{-1/2} R_4^{3/2}, \quad (77)$$

where $M_1 \equiv M/(1 M_\odot)$ and $R_4 = R/(10^4 \text{ km})$. We see that for all models, appreciable spin-orbit synchronization is achieved before mass transfer or tidal disruption. However, depending in the WD temperature, the rates of spin-orbit synchronization are different.

The basic feature of the synchronization process can be obtained using an approximate expression for the dimensionless function $F(\omega)$. We fit the local maxima of our numerical results depicted in Figures 7-9 by the function

$$F(\omega) = f\omega^5 = \hat{f}\hat{\omega}^5, \quad (78)$$

where $\hat{\omega} = \omega/(GM/R^3)^{1/2}$, and $\hat{f} \simeq 20, 200, 4 \times 10^3$ for the $T_{\text{eff}} = 10800\text{K}, 6000\text{K},$ and 3300K models, respectively. Suppose $\Omega_s \ll \Omega$ at large orbital separation. We can define the *critical orbital frequency*, Ω_c , at which spinup or synchronization becomes efficient, by equating $\dot{\Omega}$ and $\dot{\Omega}_s$ (with $\Omega_s \ll \Omega$). Note that since the orbital decay rate due to tidal energy transfer [the first term in equation (75)] is much smaller than the spinup rate $\dot{\Omega}_s$, the orbital decay is always dominated by the gravitational radiation, i.e., $\dot{\Omega} \simeq 3\dot{\Omega}_s/(2t_{\text{GW}})$. With $T_o = \bar{T}_o\Omega^4$ and $t_{\text{GW}} = \bar{t}_{\text{GW}}\Omega^{-8/3}$,

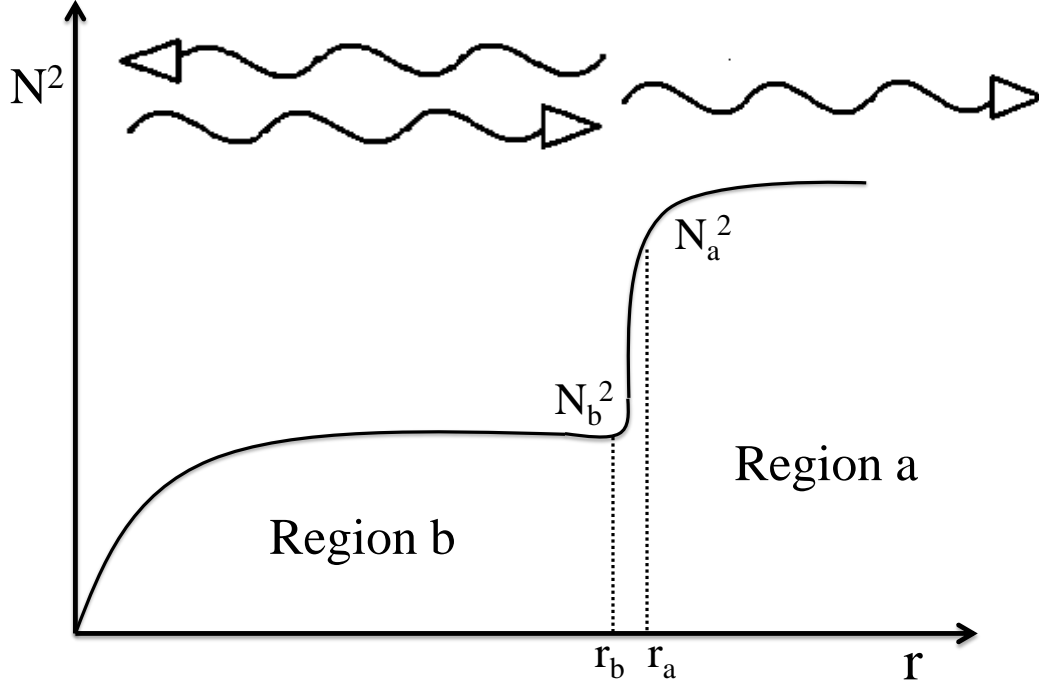


Figure 11. A diagram showing a simplified model of a white dwarf used in our analytical estimate for gravity wave excitation. The arrows indicate that region b contains both an inward and outward propagating wave, while region a contains only an outward propagating wave.

we find

$$\begin{aligned} \Omega_c &\simeq \left(\frac{3I}{64fT_o\bar{t}_{\text{GW}}} \right)^{3/16} \\ &= \left[\frac{3\kappa}{5\hat{f}} \frac{M_t^{5/3}}{M'M^{2/3}} \left(\frac{GM}{Rc^2} \right)^{5/2} \right]^{3/16} \left(\frac{GM}{R^3} \right)^{1/2} \\ &= (3.8 \times 10^{-3} \text{s}^{-1}) \left(\frac{\kappa_{0.17} M_{t1}^{5/3} M_1^{9/2}}{\hat{f} M_1' R_4^{21/2}} \right)^{3/16}, \end{aligned} \quad (79)$$

where $\kappa = 0.17\kappa_{0.17} = I/(MR^2)$, $M_1' = M'/(1M_\odot)$, and $M_{t1} = M_t/(1M_\odot)$. For $\Omega \lesssim \Omega_c$, tidal synchronization is inefficient. For $\Omega \gtrsim \Omega_c$, the spinup rate $\dot{\Omega}_s$ becomes larger than $\dot{\Omega}$ and the system will become increasingly synchronized. In fact, when $\Omega \gtrsim \Omega_c$, an approximate analytic expression for the spin evolution can be obtained by assuming *a posteriori* $(\dot{\Omega}_s - \dot{\Omega}) \ll \dot{\Omega}$. With $\dot{\Omega} \simeq 3\Omega/(2t_{\text{GW}}) \simeq \dot{\Omega}_s$, we find

$$\Omega_s \simeq \Omega - \Omega_c^{16/15} \Omega^{-1/15} \quad (\text{for } \Omega \gtrsim \Omega_c). \quad (80)$$

This expression provides an accurate representation of the numerical solutions.

Note that we can derive a similar equation as (80) for more general tidal torques. For example, assume

$$\dot{\Omega}_s = A\Omega^4(\Omega - \Omega_s)^n, \quad (81)$$

where n and A are constants. With $\dot{\Omega} = B\Omega^{11/3}$ (where B

is a constant) and assuming $\dot{\Omega}_s \simeq \dot{\Omega}$, we find

$$\Omega_s \simeq \Omega - \Omega_c \left(\frac{\Omega_c}{\Omega} \right)^{1/(3n)}, \quad (82)$$

for $\Omega \gtrsim \Omega_c$, where

$$\Omega_c = \left(\frac{B}{A} \right)^{3/(3n+1)}. \quad (83)$$

Note that our equation (80) corresponds to $n = 5$, which implies $\Omega - \Omega_s \simeq \Omega_c$ for $\Omega \gtrsim \Omega_c$. By contrast, in the equilibrium tide model (with constant lag time), $n = 1$, so $(\Omega - \Omega_s)$ changes moderately as the orbit decays.

8.2 Tidal Effect on the Orbital Decay Rate and Phase of Gravitational Waves

Figure 14 shows the tidal energy transfer rate (from the orbit to the WD) $\dot{E}_{\text{tide}} = T_0\Omega F(\omega)$. For $\Omega \lesssim \Omega_c$, $\omega \simeq 2\Omega$ (assuming $\Omega_s \ll \Omega$), we see that \dot{E}_{tide} depends on Ω in a rather erratic manner. However, when $\Omega \gtrsim \Omega_c$, efficient tidal synchronization ensures $\dot{\Omega} \simeq \dot{\Omega}_s$, or $3\Omega/2t_{\text{GW}} \simeq T_0F(\omega)/I$, and thus \dot{E}_{tide} simplifies to

$$\dot{E}_{\text{tide}} \simeq \frac{3I\Omega^2}{2t_{\text{GW}}} \quad (\text{for } \Omega \gtrsim \Omega_c). \quad (84)$$

Since $\dot{E}_{\text{tide}}/\dot{E}_{\text{GW}} \simeq 3I/(\mu a^2) \ll 1$, the orbital decay is dominated by gravitational radiation. Nevertheless, the orbital

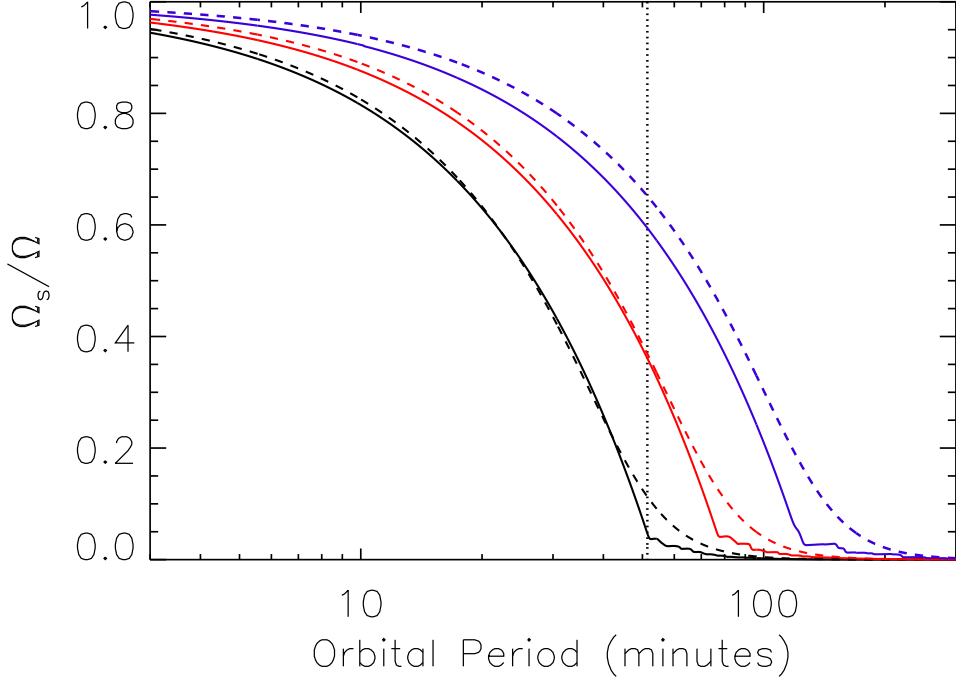


Figure 12. Evolution of the spin frequency Ω_s in units of the orbital frequency Ω as a function of the orbital period. The solid black, red, and blue lines correspond to our WD models with $T_{\text{eff}} = 10800\text{K}$, $T = 6000\text{K}$, and $T = 3300\text{K}$, respectively. The black, red, and blue dashed lines correspond to evolutions using $F = 20\hat{\omega}^5$, $F = 200\hat{\omega}^5$, $F = 4 \times 10^3\hat{\omega}^5$, respectively (these functions $F(\omega)$ approximate the like-colored WD models, see Figures 7-9). The vertical dotted line denotes the critical orbital period, $2\pi/\Omega_c$ [see equation (79)], corresponding to the black dashed line. In these evolutions, $M' = M$ and the WDs initially have $\Omega_s = 0$.

phase evolution is affected by the tidal energy transfer, and such a phase shift can be measurable for short period binaries such as the recently discovered 12 minute system SDSS J0651 (Brown et al. 2011; see Section 9). Also, low-frequency ($10^{-4} - 10^{-1}$ Hz) gravitational waveforms emitted by the binary, detectable by LISA, will deviate significantly from the point-mass binary prediction. This is in contrast to the case of neutron star binaries (NS/NS or NS/BH) studied previously (Reisenegger & Goldreich 1994; Lai 1994; Shibata 1994; Ho & Lai 1999; Lai & Wu 2006; Flanagan & Racine 2007), where the resonant mode amplitude is normally too small to affect the gravitational waveforms to be detected by ground-based gravitational wave detectors such as LIGO and VIRGO, tidal effects only become important near the NS binary merger (e.g., Lai et al. 1994; Hinderer et al. 2010).

The orbital cycle of a WD binary evolves according to

$$dN_{\text{orb}} = \frac{\Omega}{2\pi} \frac{dE_{\text{orb}}}{\dot{E}_{\text{orb}}}. \quad (85)$$

Including tidal effects in \dot{E}_{orb} , we find

$$\frac{dN_{\text{orb}}}{d \ln \Omega} = \left(\frac{dN_{\text{orb}}}{d \ln \Omega} \right)_0 \left(1 + \frac{\dot{E}_{\text{tide}}}{\dot{E}_{\text{GW}}} \right)^{-1}, \quad (86)$$

where

$$\begin{aligned} \left(\frac{dN_{\text{orb}}}{d \ln \Omega} \right)_0 &= \frac{\Omega t_{\text{GW}}}{3\pi} = \frac{5c^5}{192\pi G^{5/3} \mu M_t^{2/3} (\pi f_{\text{GW}})^{5/3}} \\ &= 2.3 \times 10^9 \left(\frac{M_{\odot}^2}{MM'} \right) \left(\frac{M_t}{2M_{\odot}} \right)^{1/3} \left(\frac{f_{\text{GW}}}{0.01 \text{ Hz}} \right)^{-5/3} \end{aligned} \quad (87)$$

is the usual result when the tidal effect is neglected ($f_{\text{GW}} = \Omega/\pi$ is the gravitational wave frequency). Thus, even though $\dot{E}_{\text{tide}}/\dot{E}_{\text{GW}} \ll 1$, the number of “missing cycles” due to the tidal effect,

$$\left(\frac{d\Delta N_{\text{orb}}}{d \ln \Omega} \right)_{\text{tide}} \simeq - \left(\frac{dN_{\text{orb}}}{d \ln \Omega} \right)_0 \frac{\dot{E}_{\text{tide}}}{\dot{E}_{\text{GW}}}, \quad (88)$$

can be significant. Since $E_{\text{tide}} \propto I$, proper modelling and detection of the missing cycles would provide a measurement of the moment of inertia of the WD.

8.3 Tidal Heating

The tidal energy transfer \dot{E}_{tide} does not correspond to the energy dissipated as heat in the WD, because some of the energy must be used to spin up the WD. Assuming rigid-body rotation, the tidal heating rate is

$$\dot{E}_{\text{heat}} = \dot{E}_{\text{tide}} \left(1 - \frac{\Omega_s}{\Omega} \right). \quad (89)$$

Figure 14 shows \dot{E}_{heat} for our three binary WD models. At large binary separations ($\Omega \lesssim \Omega_c$) when $\Omega_s \ll \Omega$, virtually all of the tidal energy transfer to the WD is dissipated as heat. At smaller separations, we have shown that the WD will retain a small degree of asynchronization. Insert-

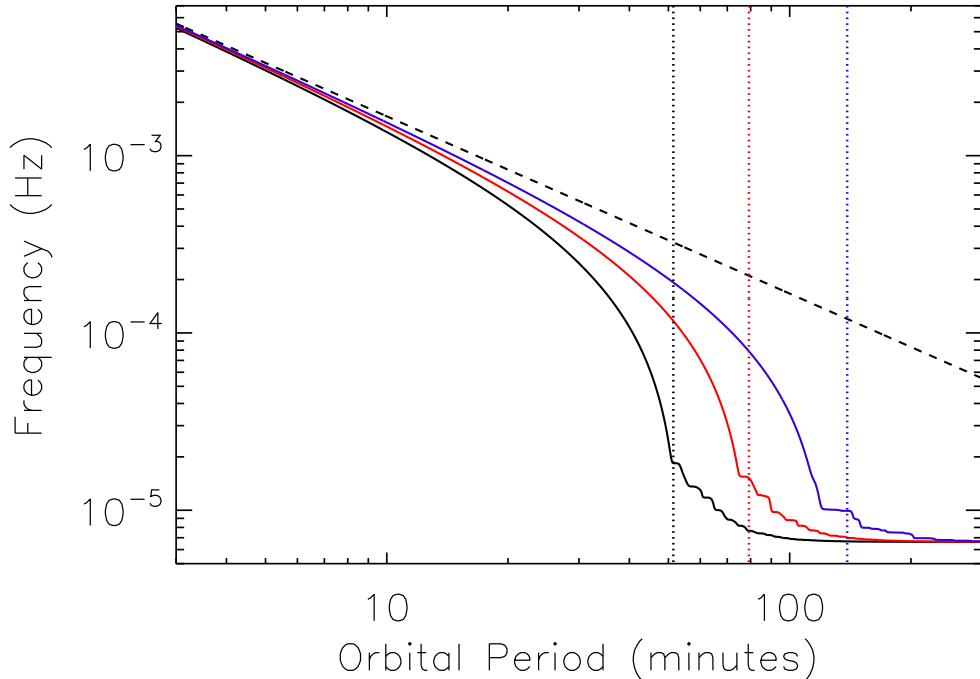


Figure 13. The spin frequency $\Omega_s/(2\pi)$ in units of Hz as a function of orbital period. The solid black, red, and blue lines correspond to our WD models with $T_{\text{eff}} = 10800\text{K}$, $T = 6000\text{K}$, and $T = 3300\text{K}$, respectively. The dashed line shows the orbital frequency, $\Omega/(2\pi)$. The dotted vertical black, red, and blue lines are the values of $2\pi/\Omega_c$ for $F = 20\hat{\omega}^5$, $F = 200\hat{\omega}^5$, $F = 4 \times 10^3\hat{\omega}^5$, respectively. In these evolutions, $M' = M$ and the WDs initially have $\Omega_s = \Omega/4$.

ing equation (80) into equation (89), we find

$$\begin{aligned} \dot{E}_{\text{heat}} &\simeq \dot{E}_{\text{tide}} \left(\frac{\Omega_c}{\Omega} \right)^{16/15} \\ &\simeq \frac{3I\Omega^2}{2t_{\text{GW}}} \left(\frac{\Omega_c}{\Omega} \right)^{16/15} \quad (\text{for } \Omega \gtrsim \Omega_c). \end{aligned} \quad (90)$$

Thus, as the orbital frequency increases, a smaller fraction of the tidal energy is dissipated as heat. Using equation (79) for Ω_c , we have

$$\begin{aligned} \dot{E}_{\text{heat}} &\simeq (6.1 \times 10^{36} \text{ erg s}^{-1}) \kappa_{0.17}^{6/5} \hat{f}^{-1/5} M_1^{29/10} \\ &\quad \times (M_1')^{4/5} R_4^{-1/10} \left(\frac{\Omega}{0.1 \text{ s}^{-1}} \right)^{18/5}. \end{aligned} \quad (91)$$

Note that \dot{E}_{heat} is relatively insensitive to \hat{f} , so its precise value is not important. Thus, tidal heating of the WD can become significant well before merger. For example, for our $T_{\text{eff}} = 10800\text{K}$ WD model (with $M = M' = 0.6M_{\odot}$, $R = 8970 \text{ km}$ and $\hat{f} \sim 20$), we find $\dot{E}_{\text{heat}} \sim 1.2 \times 10^{32} \text{ erg/s}$ at the orbital period $P = 10 \text{ min}$, much larger than the “intrinsic” luminosity of the WD, $4\pi R^2 \sigma_{\text{SB}} T_{\text{eff}}^4 = 3.3 \times 10^{30} \text{ erg/s}$. Note that \dot{E}_{heat} is mainly deposited in the WD envelope, so an appreciable fraction of \dot{E}_{tide} may be radiated, and the WD can become very bright prior to merger. The 12 minute binary SDSS J0651 (Brown et al. 2011) may be an example of such tidally heated WDs (see Section 9).

9 DISCUSSION

We have studied the tidal excitation of gravity waves in binary white dwarfs (WDs) and computed the energy and angular momentum transfer rates as a function of the orbital frequency for several WD models. Such dynamical tides play the dominant role in spinning up the WD as the binary decays due to gravitational radiation. Our calculations are based on the outgoing wave boundary condition, which implicitly assumes that the tidally excited gravity waves are damped by nonlinear effects or radiative diffusion as they propagate towards the WD surface. Unlike dynamical tides in early-type main-sequence stars, where gravity waves are excited at the boundary between the convective core and radiative envelope, the excitation of gravity waves in WDs is more complicated due to the various sharp features associated with composition changes in the WD model. We find that the tidal energy transfer rate (from the orbit to the WD) \dot{E}_{tide} is a complex function of the tidal frequency $\omega = 2(\Omega - \Omega_s)$ (where Ω and Ω_s are the orbital frequency and spin frequency, respectively; see Figures 7-9), and the local maxima of \dot{E}_{tide} scale approximately as $\Omega^5 \omega^5$. For most tidal frequencies considered, the gravity waves are excited near the boundary between the carbon-oxygen core and the helium layer (with the associated dip and sharp rise in the Brunt-Väisälä frequency profile). We have constructed a semi-analytic model that captures the basic physics of gravity wave excitation and reveals that the complex behavior of \dot{E}_{tide} as a function of the tidal frequency arises from the par-

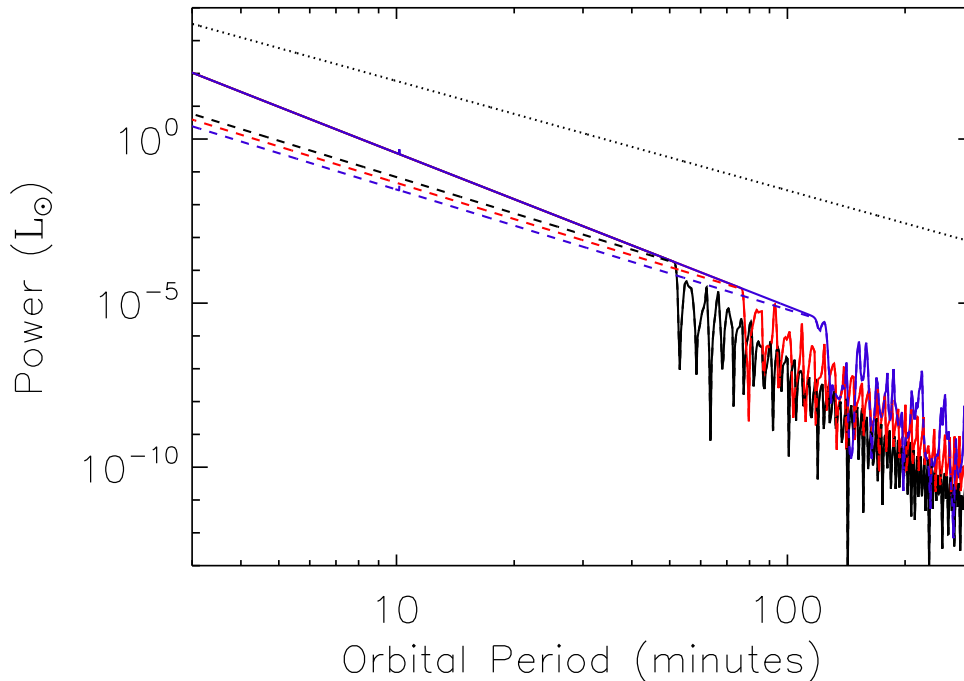


Figure 14. The tidal energy dissipation rate \dot{E}_{tide} (solid lines) and the tidal heating rate \dot{E}_{heat} (dashed lines) as a function of orbital period. The black, red, and blue lines correspond to our WD models with $T_{\text{eff}} = 10800\text{K}$, $T = 6000\text{K}$, and $T = 3300\text{K}$, respectively. Note that at small orbital periods, the \dot{E}_{tide} curves overlap for different WD models. The dotted line is the energy dissipation rate due to gravitational waves, \dot{E}_{GW} . In these evolutions, $M' = M$ and the WDs initially have $\Omega_s = 0$.

tial trapping of gravity waves in the quasi-resonance cavity provided by the carbon-oxygen core.

We have also calculated the spin and orbital evolution of the WD binary system including the effects of both gravitational radiation and tidal dissipation. We find that above a critical orbital frequency Ω_c [see equation (79)], corresponding to an orbital period of about an hour for our WD models, the dynamical tide BEGINS to drive the WD spin Ω_s towards synchronous rotation, although a small degree of asynchronization is maintained even at small orbital periods: $\Omega - \Omega_s \simeq \Omega_c (\Omega_c / \Omega)^{1/15}$ [see equation (80)]. Thus, numerical simulations of WD binary mergers should use synchronized configurations as their initial condition – these may affect the property of the merger product and possible supernova signatures.

We also show that, although gravitational radiation always dominates over tides in the decay of the binary orbit, tidal effects can nevertheless affect the orbital decay and introduce significant phase error to the low-frequency gravitational waveforms. Future detection of gravitational waves from WD binaries by LISA may need to take these tidal effects into account and may lead to measurements of the WDs' moments of inertia. Finally, we have calculated the tidal heating rate of the WD as a function of the orbital period. For $\Omega \gtrsim \Omega_c$, since the tidal dissipation rate is largely controlled by the orbital decay rate due to gravitational radiation, it is a smooth function of orbital period [see equation (90)]. We show that well before mass transfer or binary merger occurs, tidal dissipation in the WD envelope can be much larger than the intrinsic luminosity of the star. Thus,

the WD envelope may be heated up significantly, leading to brightening of the WD binary well before merger. We plan to study this issue in detail in a future paper.

The recently discovered 12 minute WD binary SDSS J0651 (Brown et al. 2011) can provide useful constraints for our theory. Applying equation (79) to this system, we find that the orbital period (12.75 minutes) is sufficiently short that both WDs are nearly (but not completely) synchronized with the orbit. Because of the orbital decay \dot{P} , the eclipse timing changes according to the relation

$$\Delta t = \dot{P} t^2 / (2P), \quad (92)$$

where t is the observing time. Gravitational radiation gives rise to $\Delta t_{\text{GW}} = 5.6\text{s} (t/1\text{yr})^2$. Using equation (84) to evaluate the orbital decay rate \dot{P}_{tide} due to tidal energy transfer, we find $\Delta t_{\text{tide}} \simeq 0.28\text{s} (t/1\text{yr})^2$ (see also Benacquista 2011). Thus, the orbital decay due to tidal effects should be measured in the near future. Also, our calculated heating rate, equation (91), indicates the SDSS J0651 WDs have suffered significant tidal heating, although to predict the luminosity change due to tidal heating requires careful study of the thermal structure of the WDs and knowledge of the location of tidal heating. We note that Piro (2011) also considered some aspects of tidal effects in SDSS J0651, but his results were based on parameterized equilibrium tide theory.

This paper, together with paper I, represents only the first study of the physics of dynamical tides in compact WD binaries, and more works are needed. We have adopted several approximations that may limit the applicability of our results. First, we have not included the effects of rotation

(e.g., the Coriolis force) in our wave equations. In addition to modifying the properties of gravity waves (they become generalized Hough waves), rotation also introduces inertial waves that can be excited once the WD spin frequency becomes comparable to the tidal frequency – this may lead to more efficient tidal energy transfer and synchronization. For example, if we parameterize the spinup rate due to various mechanisms (including inertial waves) by equation (87), the critical orbital frequency for the onset of synchronization (Ω_c) is given by equation (83). For a stronger tidal torque (larger A), Ω_c is smaller. However, the tidal heating rate at $\Omega \gtrsim \Omega_c$ becomes [cf. equation (90)]

$$\dot{E}_{\text{heat}} \simeq \frac{3I\Omega^2}{t_{\text{GW}}} \left(\frac{\Omega_c}{\Omega}\right)^{(3n+1)/(3n)}. \quad (93)$$

Thus, for stronger tidal torques, at a given orbital frequency ($\Omega \gtrsim \Omega_c$), the tidal heating rate is reduced because the WD is closer to synchronization.

Second, we have assumed that the WD rotates as a rigid body. As the tidally-excited gravity waves deposit angular momentum in the outer layer of the WD, differential rotation will develop if the different regions of the WD are not well coupled. Thus it may be that the outer layer becomes synchronized with the companion while the core rotates at a sub-synchronous rate, analogous to tidal synchronization in early-type main-sequence stars (Goldreich & Nicholson 1989). Third, we have implicitly assumed that the outgoing gravity waves are efficiently damped near the WD surface. This may not apply for all WD models or all orbital frequencies. If partial wave reflection occurs, tidal dissipation will be reduced compared to the results presented in this paper except when the tidal frequency matches the intrinsic frequency of a g-mode (cf. Paper I). More detailed studies on nonlinear wave damping (e.g., Barker & Ogilvie 2010; Weinberg et al. 2011) and radiative damping would be desirable.

Finally, we have only studied carbon-oxygen WDs in this paper. Our calculations have shown that the strength of dynamical tides depends sensitively on the detailed internal structure of the WD. Recent observations (see references in Section 1) have revealed many compact WD binaries that contain at least one low-mass helium-core WD. The temperatures of these helium-core WDs tend to be high ($T_{\text{eff}} \gtrsim 10^4\text{K}$). These observations warrant investigation of tidal effects in hot, helium-core WDs, which have significantly different internal structures from the cool, carbon-oxygen WDs considered in this paper.

ACKNOWLEDGMENTS

We thank Gilles Fontaine (University of Montreal) for providing the white dwarf models used in this paper and for valuable advice on these models. DL thanks Lars Bildsten and Gordon Ogilvie for useful discussions, and acknowledges the hospitality (Spring 2010) of the Kavli Institute for Theoretical Physics at UCSB (funded by the NSF through Grant PHY05-51164) where part of the work was carried out. This work has been supported in part by NSF grant AST-1008245.

REFERENCES

- Alexander, M.E. 1973, *Astrophys. Space Sci.*, 23, 459
 Barker, A., Ogilvie, G. 2010, *MNRAS*, 404, 1849
 Barker, A., Ogilvie, G. 2011, arXiv:1102.0861
 Benacquista, M. 2011, *ApJ*, 740, L54
 Brassard, P., Fontaine, G., Wesemael, F., Kawaler, S.D., Tassoul M. 1991, *ApJ*, 367, 601
 Brown, R.B., Kilic, M., Hermes, J.J., Allende Prieto, C., Kenyon, S.J., Winget, D.E. 2011, arXiv:1107.2389v1
 Darwin, G.H. 1879, *Phil. Trans. Roy. Soc.*, 170, 1
 Di Stefano, R. 2010, *ApJ*, 719, 474
 Flanagan, E., Racine, E. 2007, *Phys. Rev. D*75, 044001
 Fuller, J., Lai, D. 2011, *MNRAS*, 412, 1331
 Gilfanov, M., Bogdan, A., 2010, *Nature*, 463, 924
 Goldreich, P., Nicholson, P., 1989, *ApJ*, 342, 1079
 Golreich, P., & Soter, S. 1966, *Icarus*, 5, 375
 Goodman, J., Dickson, E.S., 1998, *ApJ*, 507, 938
 Hinderer, T., Lackey, B.D., Lang, R.N., Read, J.S. 2010, *Phys. Rev. D*81, 123016
 Ho, W.C.G., Lai, D. 1999, *MNRAS*, 308, 153
 Hut, P. 1981, *A&A*, 99, 126
 Iben, I., Tutukov, A. 1984, *ApJS*, 54, 335
 Iben, I., Tutukov, A., Fedorova, A. 1998, *ApJ*, 503, 344
 Kilic, M., Brown, W.R., Kenyon, S.J., Allende Prieto, C., Andrews, J., Kleinman, S.J., Winget, K.I., Winget, D.E., Hermes, J.J. 2011, arXiv:1103.2354
 Kulkarni, S.R., van Kerkwijk, M.H., 2010, *ApJ*, 719, 1123
 Lai, D. 1994, *MNRAS*, 270, 611
 Lai, D., Rasio, F.A., Shapiro, S.L. 1994, *ApJ*, 420, 811
 Lai, D., Wu, Y. 2006, *Phys. Rev. D*74, 024007
 Loren-Aguilar, P., Isern, J., Garcia-Berro, E. 2009, *AA*, 500, 1193
 Maoz, D., Sharon, K., Gal-Yam, A. 2010, *ApJ*, 722, 1979
 Marsh, T. 2011, arXiv:1101.4970
 Mullally, F., Badenes, C., Thompson, S.E., Lupton, R. 2009, *ApJ*, 707, L51
 Nelemans, G. 2009, *Class. Quantum Grv.*, 26, 094030
 Ogilvie, G.I., Lin, D.N.C. 2007, *ApJ*, 661, 1180
 Pakmor, R., Kromer, M., Ropke, F.K., Sim, S.A., Ruiter, A.J., Hillebrandt, W. 2010, *Nature*, 463, 61
 Pakmor, R., Hachinger, S., Ropke, F.K., Hillebrandt, W., 2011, *AA*, 528, A117
 Piro, T. 2011, *ApJ*, 740, L53
 Press, W.H., Teukolsky, S.A., Vetterling, W.T., Flannery, B.P. 1998, *Numerical Recipes* (Cambridge Univ. Press)
 Reisenegger, A., Goldreich, P. 1994, *ApJ*, 426, 688
 Segretain, L., Chabrier, G., Mochkovitch, R. 1997, *ApJ*, 481, 355
 Shibata, M. 1994, *Prog. Theo. Phys.*, 91, 871
 Steinfadt, J., Kaplan, D.L., Shporer, A., Bildsten, L., Howell, S.B. 2010, *ApJ*, 716, L146
 Unno, W., Osaki, Y., Ando, H., Saio, H., Shibahashi, H. 1989, *Nonradial Oscillations of Stars* (University of Tokyo Press)
 Van Kerkwijk, M.H., Chang, P., Justham, S. 2010, *ApJL*, 722, 157
 Webbink, R.F. 1984, *ApJ*, 277, 355
 Weinberg, N., Arras, P., Quataert, E., Burkart, J. 2011, arXiv:1107.0946v1
 Willems, B., Deloye, C.J., Kalogera, V. 2010, *ApJ*, 713, 239
 Zahn, J.P. 1975, *AA*, 41, 329
 Zahn, J.P. 1977, *AA*, 57, 383

APPENDIX A: CALCULATION WITH MASSIVE STAR MODEL

To test the accuracy of our numerical calculations and especially the importance of self-consistency in real stellar models, we compute the tidal response of several toy models. The

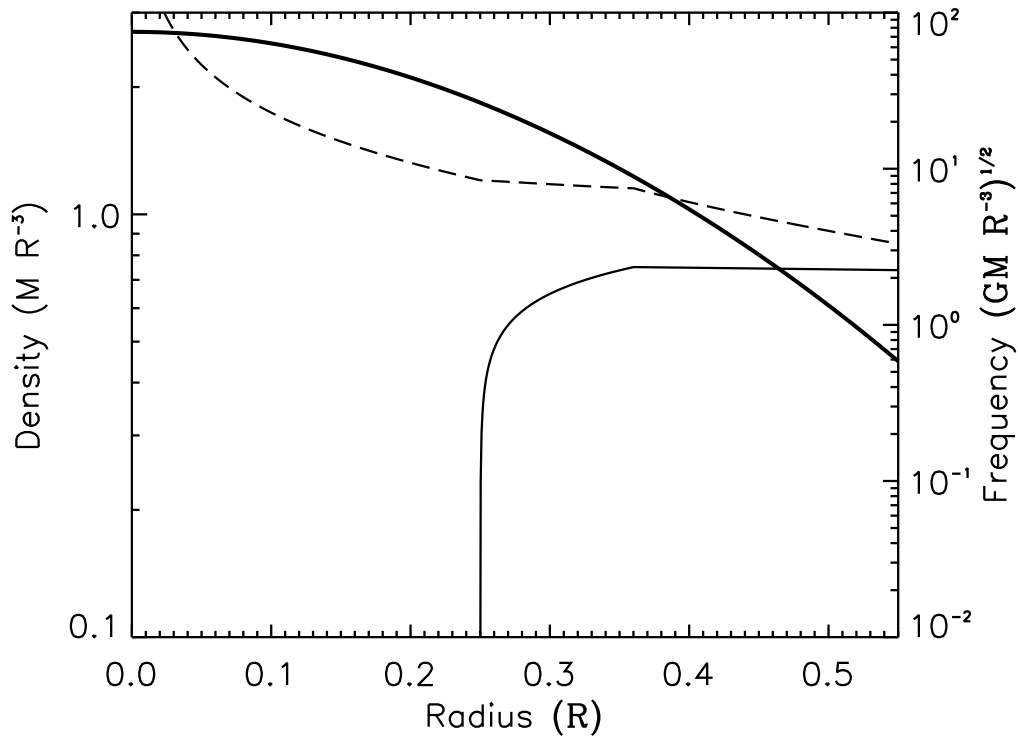


Figure A1. The square of the Brünt-Vaisälä (thin solid line) and Lamb (dashed line) frequencies (for $l = 2$), in units of GM/R^3 , as a function of the normalized radius in a simple massive star model. Also plotted is the stellar density profile (thick solid line) in units of M/R^3 . The model has an inner convection zone extending to $r = 0.25R$. The stellar properties are only plotted out to $r = 0.6R$, where an outgoing wave boundary condition is adopted in our calculation of the tidal excitation.

first toy model we employ is shown in Figure A1 and is meant to mimic a massive early-type star. The model contains an inner convection zone surrounded by a thick radiative envelope. The convection zone extends to $r = 0.25R$, beyond which the value of N^2 rises linearly to $N^2 \approx 8GM/R^3$. Dynamical tides in such massive stars have been studied by Zahn (1975, 1977) and Goldreich & Nicholson (1989), who showed that the dominant effect arises from the gravity waves launched at the core-envelope boundary, which then propagate outwards and eventually dissipate near the stellar surface. Zahn (1975) derived an analytic solution for the wave amplitude and the corresponding tidal torque. Although our model does not contain some of the details exhibited by realistic massive star models, it does capture the most important features. We can compare our result with Zahn's to calibrate our numerical method and to assess the degree of self-consistency required to produce reliable results for the tidal torque.

Figure A2 shows an example of our numerical results for the dynamical tides generated in a massive star by a companion, for a given tidal frequency $\omega = 2\Omega = 2.3 \times 10^{-2}$ (in units where $G = M = R$). We see that gravity waves are excited at the base of the radiative zone where N^2 begins to rise above zero. A net energy flux $\dot{E} = \Omega \dot{J}_z = \Omega(GM^2R^5/a^6)F(\omega)$ flows outwards toward the stellar surface. Figure A3 shows our numerical result of the dimensionless function $F(\omega) \equiv \dot{J}_z/T_o$ [see equation (42)], evaluated at the outer boundary, as a function of the tidal frequency ω .

The result can be fitted by $F(\omega) \propto \omega^{8/3}$, in agreement with the scaling found by Zahn (1975).

The power-law scaling of the energy flux can be derived using the method of Goldreich & Nicholson (1989). Assume $|\xi_{\perp}^{\text{dyn}}| \approx \xi_{\perp}^{\text{eq}}$ at $r = r_{c+}$, which is located one wavelength above the convective boundary ($r = r_c$). From the dispersion relation (27), we find that the Brünt-Vaisälä frequency at r_{c+} is given by (for $l = 2$)

$$N(r_{c+}) \approx \left(\frac{dN^2}{dr} r_c \right)^{1/3} \omega^{1/3}. \quad (\text{A1})$$

Using $\xi_{\perp}^{\text{eq}} \simeq -[1/(6r)](Ur^2/g)' \simeq -U/(2g)$, we evaluate equation (41) to find

$$\dot{E} \approx \frac{3\pi\sqrt{6}}{10} \left(\frac{M'}{M_t} \right)^2 \frac{\rho r^7 \Omega^5 \omega^{8/3}}{g^2 (dN^2/d \ln r)^{1/3}}. \quad (\text{A2})$$

where $M_t = M + M'$, and all the quantities (ρ , r , g , and dN^2/dr) are evaluated at $r = r_{c+} \simeq r_c$. The scaling of this estimate nearly agrees Goldreich & Nicholson (1989), who obtained $\dot{E}_r \propto \Omega^4 \omega^{11/3}$, where \dot{E}_r is the energy flux carried by outgoing gravity waves in the rotating frame of the star, not the total energy transfer rate from the orbit. These two energy transfer rates are related by $\dot{E} = \Omega \dot{J}_z = 2\Omega \dot{E}_r / \omega$. Goldreich & Nicholson (1989) estimates $dN^2/dr \approx g/H \approx g/r$, and with $g \simeq 4\pi G \bar{\rho} r / 3$ ($\bar{\rho}$ is the mean density interior

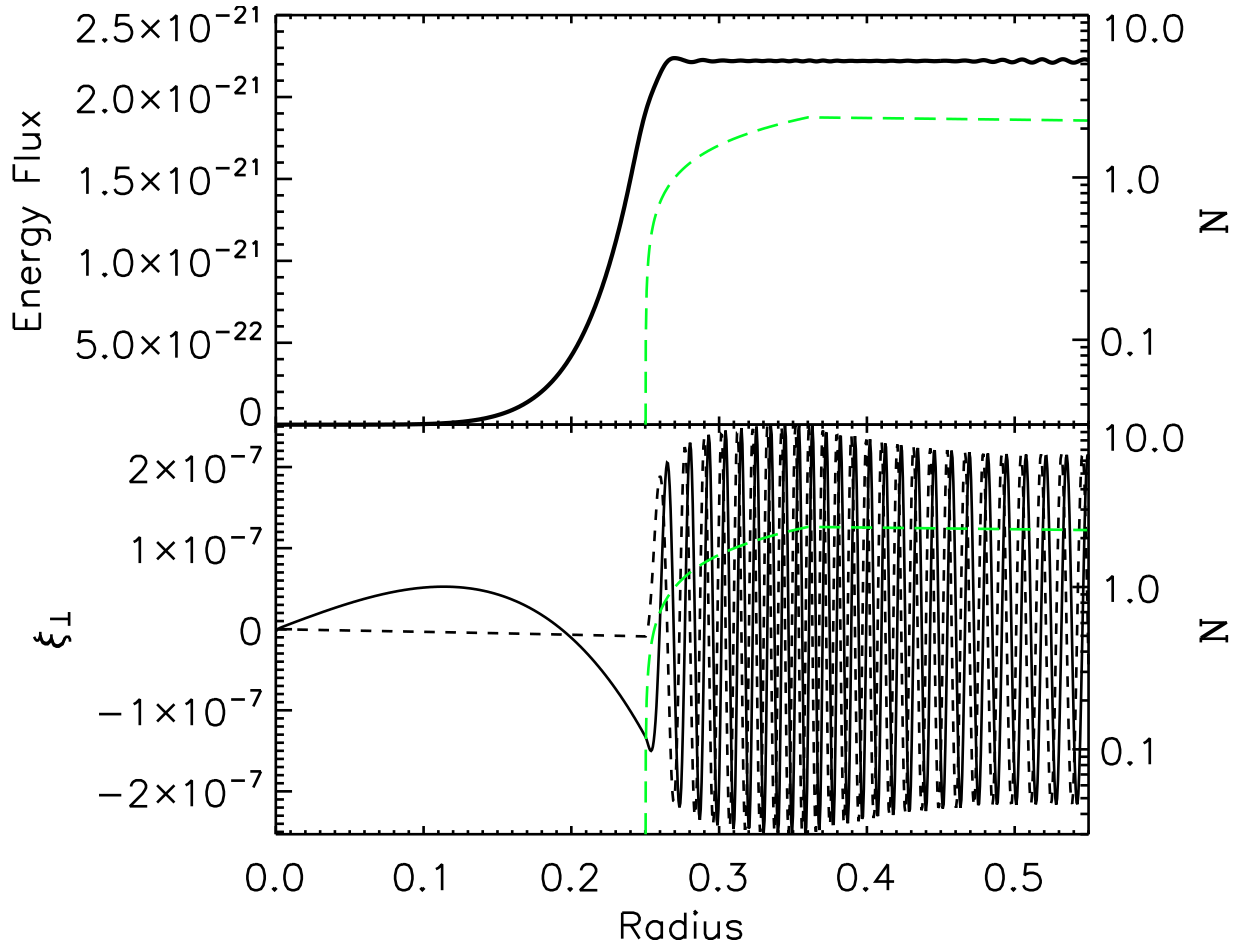


Figure A2. Dynamical tide in a massive star (based on the toy model depicted in Figure A1) driven by a companion of mass $M' = M$, with the tidal frequency $\omega = 2.3 \times 10^{-2}$. Top: The energy flux (dark solid line) $\dot{E} = \Omega \dot{J}_z$ as a function of radius, with \dot{J}_z calculated from equation (39). All values are plotted in units of $G = M = R = 1$. Bottom: The real part of ξ_{\perp}^{dyn} (dark solid line) and imaginary part of ξ_{\perp}^{dyn} (dashed line) as a function of stellar radius. The value of N has been plotted in green (light solid line) in both panels. In this model, the energy flux rises to its final value just outside of the convective zone, showing that the wave is excited at this location.

to r_c), equation (A2) becomes

$$\dot{E} \approx 0.08 \left(\frac{M'}{M_t} \right)^2 \frac{\rho r^5 \Omega^5 \omega^{8/3}}{(G\bar{\rho})^{7/3}}. \quad (\text{A3})$$

The value of $F(\omega)$ based on equation (A2) is plotted in Figure A3. Compared to our numerical results, we see that equation (A2) overestimates $F(\omega)$ by an order of magnitude [by contrast, equation (A3) would overestimate $F(\omega)$ by more, since for our toy stellar model $dN^2/d\ln r \gg g/r$]. From our numerical results, we find that the dynamical part of the tide only reaches an amplitude of $\xi_{\perp}^{\text{dyn}} \approx \xi_{\perp}^{\text{eq}}/4$. If we had used this wave amplitude in our estimate, equation (A2) would be a factor of 16 smaller and would provide an accurate approximation to $F(\omega)$ at all frequencies considered.

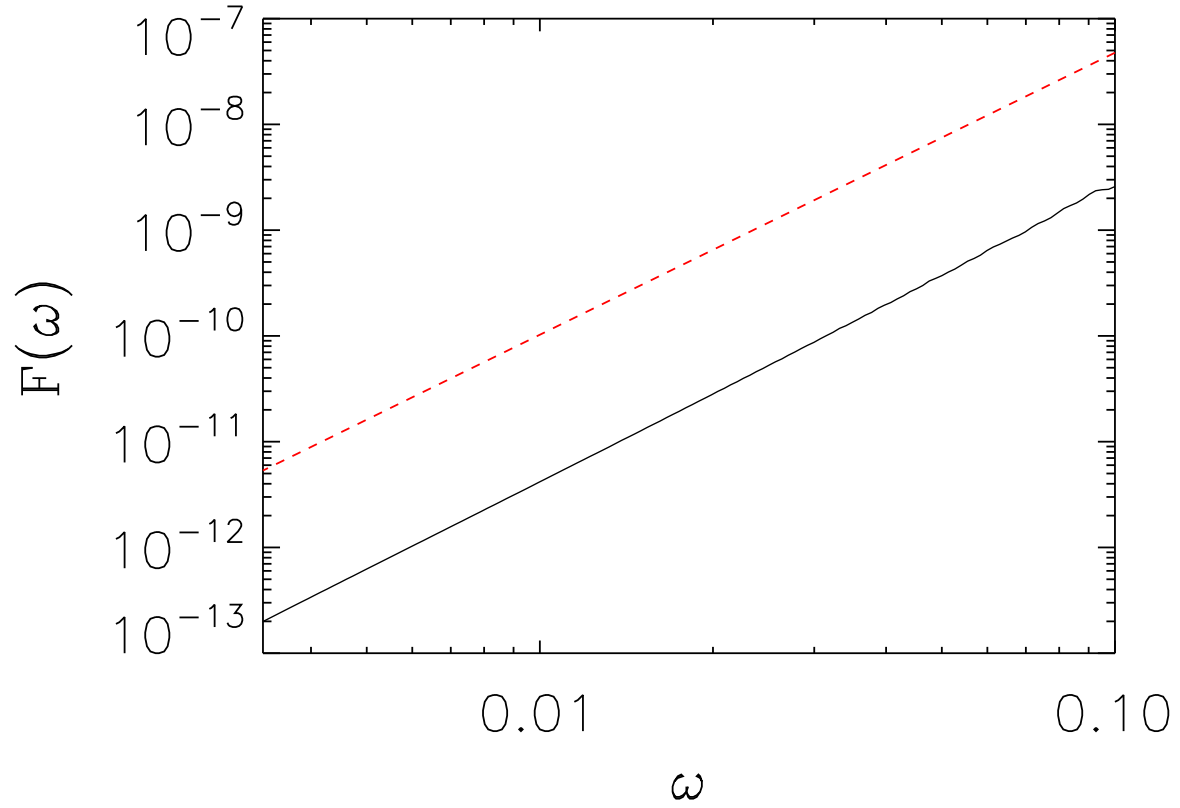


Figure A3. The dimensionless tidal torque $F(\omega) = \dot{J}_z/T_o$ [see equation (42)] carried by the outgoing gravity wave as a function of the tidal frequency ω (solid line). The analytical estimate from equation (A2) is also plotted (dashed line). The frequency is in units of $G = M = R = 1$. The small wiggles at high frequencies are likely due to the slight inaccuracy of our implementation of the outer boundary condition due to the neglected terms which become non-negligible at higher tidal frequencies.